

# Absolute kinematics of radio source components in the complete S5 polar cap sample

## II. First and second epoch maps at 15 GHz

M.A. Pérez-Torres<sup>1,2</sup>, J.M. Marcaide<sup>3</sup>, J.C. Guirado<sup>3</sup>, and E. Ros<sup>4</sup>

<sup>1</sup> Istituto di Radioastronomia, Via P. Gobetti 101, 40129 Bologna, Italy

<sup>2</sup> Instituto de Astrofísica de Andalucía (CSIC), Apdo. Correos 3004, E-18080 Granada, Spain

<sup>3</sup> Departament d'Astronomia i Astrofísica, Universitat de València, E-46100 Burjassot, València, Spain

<sup>4</sup> Max-Planck-Institut für Radioastronomie, Auf dem Hügel 69, D-53121 Bonn, Germany

Submitted: 10 March 2004 / Accepted: 27 July 2004

**Abstract.** We observed the thirteen extragalactic radio sources of the complete S5 polar cap sample at 15.4 GHz with the Very Long Baseline Array, on 27 July 1999 (1999.57) and 15 June 2000 (2000.46). We present the maps from those two epochs, along with maps obtained from observations of the 2 cm VLBA survey for some of the sources of the sample, making a total of 40 maps. We discuss the apparent morphological changes displayed by the radio sources between the observing epochs. Our VLBA observations correspond to the first two epochs at 15.4 GHz of a program to study the absolute kinematics of the radio source components of the members of the sample, by means of phase delay astrometry at 8.4 GHz, 15.4 GHz, and 43 GHz.

Our 15.4 GHz VLBA imaging allowed us to disentangle the inner milliarcsecond structure of some of the sources, thus resolving components that appeared blended at 8.4 GHz. For most of the sources, we identified the brightest feature in each radio source with the core. These identifications are supported by the spectral index estimates for those brightest features, which are in general flat, or even inverted. Most of the sources display core-dominance in the overall emission, as given by the core-to-extended ratio in the 15.4 GHz frame,  $Q$ . We find that three of the sources have their most inverted spectrum component shifted with respect to the origin in the map, which approximately coincides with the peak-of-brightness at both 15.4 GHz and 8.4 GHz.

**Key words.** astrometry – techniques: interferometric – quasars: general – BL Lacertae objects: general

### 1. Introduction

This paper is the second of a series aimed at conducting absolute kinematics studies of a complete sample of extragalactic radio sources, using astrometry techniques. The sample consists of the thirteen sources from the S5 polar cap sample, selected by Eckart et al. (1986, 1987) from the S5 survey (Kühr et al. 1981), that satisfy the following criteria: (i)  $\delta \geq 70^\circ$ , (ii)  $|b_{\text{II}}| \geq 10^\circ$ , (iii)  $S_{5\text{ GHz}} \geq 1\text{ Jy}$  at the epoch of the survey, and (iv)  $\alpha_{2.7, 5\text{ GHz}} \geq -0.5$  ( $S \sim \nu^{+\alpha}$ ). Hereafter, we shall refer to those thirteen radio sources as “the complete S5 polar cap sample”.

We described the goals of our astrometric program in Ros et al. (2001, hereafter Paper I), and presented 8.4 GHz VLBA maps obtained at two different epochs, 1997.93 and 1999.41. We refer the reader to that paper for further de-

tails. We recall here that this ongoing astrometric program is intended to test the absolute kinematics of the innermost regions of the sources of the complete S5 polar cap sample, with precisions better than  $\sim(20\text{ to }100)\mu\text{as}$ , depending on the observing frequency. We expect to obtain such accurate results only after the mapping and astrometric reduction of our observations are completed. The determination of the detailed kinematics of the compact components of the complete S5 polar cap sample will probably be a decisive element in our understanding of the activity around the cores of these compact radio sources, and in a definitive test of the standard jet model.

We present here our 15.4 GHz maps obtained with the Very Long Baseline Array on 1999.57 and 2000.46. We also present maps obtained from observations of some of the sources of the complete sample that are targets of the 2 cm VLBA survey (Kellermann et al. 1998, Zensus

Send offprint requests to: M.A. Pérez-Torres, torres@iaa.es

et al. 2002). We discuss in detail the apparent changes in the brightness distribution of some of the radio sources during the time covered by the 15.4 GHz observations, as well as a comparison with the results presented at 8.4 GHz (Paper I). Throughout the paper, we use a Hubble constant  $H_0=65 h \text{ km s}^{-1} \text{ Mpc}^{-1}$  and a deceleration parameter  $q_0=0.5$ .

## 2. Observations

We observed the complete S5 polar cap sample at 15.4 GHz on 27 July 1999 (epoch 1999.57) and on 15 June 2000 (epoch 2000.46) with the VLBA, each time for 24 hours. For the first epoch, we used the standard VLBA recording mode 128–8–1 (data rate of 128 Mbps, recording in 8 IFs of 16 channels each), in left circular polarization, thus yielding a total bandwidth of 64 MHz. For scheduling reasons, in our second epoch we used the standard recording VLBA mode 64–4–1 (data rate of 64 Mbps, recording in 4 IFs of 8 channels each), also in left circular polarization, yielding a total bandwidth of 32 MHz. All data were correlated at the VLBA Array Operations Center of the National Radio Astronomy Observatory (NRAO) in Socorro, New Mexico, using a basic integration time of 4 s. All radio sources were detected and provided fringes for all baselines. We cycled around in groups of three or four radio sources, with duty cycles of about 5 min. Every scan was 55 s long, and antenna slew times were  $\lesssim 20$  s. We replaced one or two members of the group of observed sources by new ones every two hours approximately, until all thirteen sources of the sample had been observed. We tracked the clock behaviour—of relevance for the astrometric analysis—by including some scans of BL 0454+844 in all groups observed during the first (second) half of the experiment on 27 July 1999 (15 June 2000), and of BL 2007+777 in all groups observed during the second (first) half.

After fringe-fitting the correlator output, we obtained correlation amplitudes for each source. We calibrated the visibility amplitudes in a standard manner, using the antenna gain and system temperature information provided by each station. We then used the Caltech VLBI Package (Pearson 1991) and the difference mapping software DIFMAP (Shepherd et al. 1994) to obtain the radio images shown in this paper.

## 3. Imaging results

We imaged all thirteen radio sources using standard hybrid mapping techniques. We found minor amplitude calibration problems for the Saint Croix antenna at epoch 1999.57; the noise level was high for most of the observing run. Nevertheless, we used the data for Saint Croix, since it provides long baselines, and hence high resolution. We show the maps obtained in Figs. 2 through 14. In all

figures, east is left, and north is up. We list the main parameters of those maps in Tables 1 and 3.

We also present images of several sources of the S5 polar cap sample obtained from observations of the VLBA 2 cm Survey that were relatively close in time to our observations. We used the same data reduction and standard hybrid mapping techniques that were used with our own data. To distinguish the 2 cm VLBA survey maps from ours, we have labelled the latter “2 cm survey”.

We now proceed to discuss the apparent morphological changes displayed by each of the radio sources of the complete polar cap sample, as seen from 15.4 GHz VLBA observations made in 1999.57 and 2000.46, complemented with maps of some of the sources, which we obtained from observations of the 2 cm VLBA Survey (Kellermann et al. 1998; Zensus et al. 2002; see also <http://www.nrao.edu/2cmsurvey>). To quantify the morphological changes displayed by the radio sources, we used the tasks MODFIT and ERFIT of the Caltech package (Pearson 1991) to fit the visibility data to a model of elliptical components with Gaussian brightness profiles. Those models are listed in Tables 2 and 3.

We compare our observations with those taken at 8.4 GHz with the VLBA in 1997.93, and in particular in 1999.41 (very close to our first epoch, 1999.57), and presented in Paper I. These yield the spectral index,  $\alpha$  ( $S \sim \nu^\alpha$ ) for those 15.4 GHz source components that have clear counterparts at 8.4 GHz. We refer the reader to Paper I for a comprehensive discussion of historical details for each radio source.

We also show in Fig. 3.1 the distance to the core for sources of the S5 polar cap sample that were observed at least three times, and in Table 4 we present proper motions obtained from model fitting source component positions at different epochs. We list proper motions only for those components that were identified in at least three epochs, and whose proper motion exceeded  $1\sigma$ .

### 3.1. QSO 0016+731

The source QSO 0016+731 (Fig. 2,  $z=1.781$ ) shows at 15.4 GHz a core-jet structure at an angle of  $\sim 130^\circ$ . The modeling of the radio source provides a good fit with three components: a compact, strong one (UA), which likely corresponds to the core, and two extended, weak components (UB and UC), directed to the east-southeast, and which correspond to the jet. The total flux density increased significantly from 647 mJy to 817 mJy (26% change) between our two observing epochs. The corresponding monochromatic luminosity is  $L_{15 \text{ GHz}} \approx (1.3 \text{ to } 1.6) \times 10^{39} \text{ W}$ . The increase in the total flux density of the source was due to a strong increment in the flux of the westernmost component (UA, the brightest feature in Fig. 2). Correspondingly, the observed, uncorrected ratio of the core flux density to the extended flux density in

**Table 1.** Map parameters for sources of the complete S5 polar cap sample at 15.4 GHz.

Source	Epoch 1999.57					Epoch 2000.46				
	Beam FWHM <sup>a</sup>		$S_{\text{peak}}$ [mJy/beam]	$S_{\text{tot}}$ <sup>(b)</sup> [mJy]	rms level <sup>c</sup> [mJy/beam]	Beam FWHM <sup>a</sup>		$S_{\text{peak}}$ [mJy/beam]	$S_{\text{tot}}$ <sup>(b)</sup> [mJy]	rms level <sup>c</sup> [mJy/beam]
	Size [mas]	P.A.				Size [mas]	P.A.			
<b>QSO 0016+731</b>	0.619×0.396	6°4	487	647	0.5	0.643×0.392	6°9	694	817	0.6
<b>QSO 0153+744</b>	0.860×0.352	-6°9	163	316	1.0	0.853×0.345	-4°9	169	312	0.7
<b>QSO 0212+735</b>	0.899×0.371	-3°3	1025	2529	0.5	0.869×0.366	-3°4	1032	2507	0.6
<b>BL 0454+844</b>	0.425×0.362	57°5	59	120	0.4	0.393×0.370	70°9	71	131	0.4
<b>QSO 0615+820</b>	0.451×0.401	22°6	129	434	0.7	0.475×0.392	16°4	148	410	0.7
<b>BL 0716+714</b>	0.853×0.344	-4°9	1024	1107	0.8	0.845×0.326	-2°7	968	1051	0.7
<b>QSO 0836+710</b>	0.885×0.345	-15°9	1259	1766	0.8	0.898×0.336	-12°5	1147	1728	0.6
<b>QSO 1039+811</b>	0.621×0.390	-18°3	737	926	0.6	0.546×0.365	-11°7	584	826	0.9
<b>QSO 1150+812</b>	0.626×0.310	-39°0	316	946	0.8	0.659×0.345	-37°2	358	907	0.6
<b>BL 1749+701</b>	1.044×0.359	-7°3	229	382	0.7	1.268×0.405	-16°8	261	405	0.9
<b>QSO 1803+784</b>	0.571×0.374	-3°0	1965	2878	0.8	0.533×0.426	15°3	1524	2313	0.9
<b>QSO 1928+738</b>	1.090×0.376	15°9	1492	3006	1.0	1.371×0.394	8°1	1214	2889	0.8
<b>BL 2007+777</b>	0.487×0.429	-30°1	384	825	0.4	0.488×0.422	-49°1	680	1258	0.5

<sup>a</sup> The restoring beam is an elliptical Gaussian with full-width-half-maximum (FWHM) axes  $a \times b$ . For each source, the position angle (P.A.) stands for the direction of the major axis measured north through east.

<sup>b</sup> Total flux density recovered in the hybrid mapping process.

<sup>c</sup> Contours in the maps of the figures shown in Sects. 3.1 to 3.13 are the tabulated rms values times  $(-3, 3, 3\sqrt{3}, 9, \dots)$ .

the 15.4 GHz frame,  $Q$ , increased from 4 up to 11 between 1999.57 and 2000.99. Our map of QSO 0016+731 from observations of the VLBA 2cm survey on 2000.99 (bottom panel in Fig. 2) shows that the total flux density of the source did not change significantly for over six months ( $\lesssim 1\%$  decrement).

In Paper I, the lower resolution of the observations prevented us from clearly distinguishing which component of QSO 0016+731 (either XA, or XB in Fig. 2) could be identified with the core, a much easier task at 15.4 GHz. We suggest that component UA in our maps corresponds to component XA in Paper I. In addition, it seems clear that component XB is indeed a blend of two components, UB and UC. Component XC has no counterpart in our maps. The second observing epoch at 8.4 GHz (1999.41) was close in time to our first observing epoch at 15.4 GHz (1999.57). Assuming that the 8.4 GHz flux density of the source did not change between 1999.41 and 1999.57, we obtain a global spectral index,  $\alpha$ , of 0.89. The spectral index of component UA/XA is much more inverted,  $\alpha=1.99$ , while  $\alpha = -0.68$  for the jet structure (UB+UC/XB).<sup>1</sup>

<sup>1</sup> We have kept the name convention used in Paper I. Thus, “UA” represents the first component (“A”) at the observing frequency band (“U”, corresponding to 15.4 GHz). We have also tried to assign to a given feature of a source the same name as used in Paper I. However, this has not always been possible. For example, we have no component labeled UE, nor UF for QSO 0212+735 (see Sect. 3.3). This means we found no counterpart at 15.4 GHz for components XE and XF.

### 3.2. QSO 0153+744

QSO 0153+744 (Fig. 3,  $z=2.341$ ) is a one-sided radio source (e.g., Hummel et al. 1988), whose 15.4 GHz VLBA emission is dominated by two components, UA and UB, separated by  $\sim 10$  mas ( $\sim 61 h^{-1}$  pc). The main component, UA (likely the core), is composed of three sub-components, UA1, and UA2 and UA3 (the innermost regions of the jet). UA2 and UA3 trace a smooth change in the direction of the jet, changing from  $65^\circ \pm 3^\circ$  at a distance  $r = (0.65 \pm 0.05)$  mas [ $\sim (3.6$  to  $4.2) h^{-1}$  pc], to  $88^\circ \pm 8^\circ$  at a distance  $r = (1.35 \pm 0.05)$  mas. No emission is detected above  $3\sigma$  (3 mJy), up to a distance of  $\sim 10$  mas ( $\sim 61 h^{-1}$  pc), where component UB traces the outermost regions of the jet. At this distance, the jet is at an angle  $\sim 150^\circ$ .

The total flux density stayed remarkably stable between 1999.57 and 2000.46, decreasing from  $(316 \pm 3)$  mJy to  $(312 \pm 2)$  mJy. It decreased by 8% between 2000.46 and 2000.99, down to  $(288 \pm 2)$  mJy, implying  $L_{15 \text{ GHz}} \approx (1.0$  to  $1.1) \times 10^{39}$  W. At all three epochs, component UA contributed  $\approx 80\%$  to the total flux density, while component UB contributed the remaining  $\approx 20\%$ . The brightest sub-component of UA, UA1, slightly increased its flux density in spite of the total flux decrease. On the contrary, both UA2 and UA3 continued to fade between 1999.57 and 2000.99 (e.g., UA2 decreased its flux density by  $\approx 50\%$ ). The value of  $Q$  (taken to be the ratio of emission from UA1 to the rest of the emission) increased from 1.26 in 1999.57 to 1.94 in 2000.99, indicating that the compact core marginally dominates the total emission, and tended to increase this dominance.

**Table 2.** Elliptical Gaussian component model parameters for the radio sources of the complete S5 polar cap sample.

Source	Comp.	Epoch 1999.57						Epoch 2000.46					
		$S$ [mJy]	$r$ [mas]	$\theta$	$a$ [mas]	$b/a$	$\phi$	$S$ [mJy]	$r$ [mas]	$\theta$	$a$ [mas]	$b/a$	$\phi$
0016+731	UA	510±2	0	–	0.11±0.05	0.75±0.06	–61±7	718±2	0	–	0.09±0.00	0.65±0.09	–94±4
	UB	96±13	0.80±0.06	137±1	0.57±0.04	0.89±0.05	107±16	59±15	0.77±0.06	139±1	0.61±0.04	0.96±0.17	17±258
	UC	43±13	1.32±0.06	124±1	0.84±0.07	0.82±0.09	155±31	41±14	1.42±0.06	129±2	0.75±0.15	0.81±0.18	105±19
0153+744	UA1	176±13	0	–	0.12±0.07	0.15±1.41	63±21	188±2	0	–	0.12±0.01	0.54±5.93	81±12
	UA2	50±17	0.58±0.09	70±2	0.51±0.22	0.33±0.21	–80±19	38±4	0.65±0.09	65±1	0.48±0.08	0.32±1.32	89±10
	UA3	25±5	1.29±0.09	83±1	0.63±0.08	0.33±0.11	139±9	22±2	1.38±0.09	95±2	1.00±0.13	0.33±0.07	–23±5.4
	UB1	43±4	10.27±0.09	153±1	1.14±0.12	0.87±0.12	–66±22	36±5	10.13±0.09	154±1	1.35±0.12	0.65±0.12	34±10
	UB2	20±4	11.14±0.09	151±1	0.73±0.12	0.59±0.10	–32±9	30±5	11.02±0.09	151±1	0.90±0.12	0.66±0.15	–73±18
0212+735	UA	1123±71	0.55±0.09	–49±2	0.25±0.02	0.43±0.03	–52±3	1233±31	0.59±0.09	–44±2	0.30±0.01	0.31±0.06	–60±3
	UB1	674±97	0	–	0.52±0.10	0.53±0.14	–28±6	411±118	0	–	0.59±0.10	0.48±0.13	–55±6
	UB2	595±160	0.26±0.09	+90±7	0.29±0.03	0.82±0.14	–172±8	708±111	0.25±0.09	+70±11	0.32±0.03	0.89±0.04	–141±38
	UC	88±17	0.90±0.16	97±2	1.75±0.37	0.44±0.11	103±5	74±13	0.90±0.12	93±2	1.37±0.23	0.43±0.11	89±5
	UD	43±4	2.51±0.09	101±1	0.79±0.06	0.46±0.11	118±6	47±3	2.49±0.09	99±1	0.95±0.08	0.66±0.06	132±7
	UG	26±2	13.81±0.09	93±1	1.87±0.18	0.41±0.12	111±6	32±3	13.71±0.09	92±1	2.29±0.23	0.43±0.09	115±6
	UA	93±5	0	–	0.37±0.01	0.49±0.04	–1±2	121±1	0	–	0.35±0.01	0.27±0.03	–2±1
0454+844	UB <sup>a</sup>	20±5	0.49±0.08	137±3	0.65±0.12	0.73±0.16	–31±19						
	UC <sup>a</sup>	10±1	1.71±0.08	172±1	1.01±0.09	0.58±0.08	–48±8	19±1	1.15±0.08	158±1	1.77±0.09	0.31±0.04	–31±4
	UA	221±8	0	–	0.34±0.01	0.89±0.03	–18±19	242±4	0	–	0.41±0.01	0.46±0.05	138±1
0615+820	UA2	131±6	0.58±0.05	–73±2	1.35±0.03	0.50±0.04	37±2	71±3	0.84±0.05	–99±1	1.35±0.04	0.31±0.03	17±2
	UA3	80±4	0.71±0.05	–147±1	0.25±0.04	0.14±0.32	–119±9	107±3	0.74±0.05	–152±1	0.25±0.03	0.10±0.93	40±4
	UA	1058±5	0	–	0.17±0.01	0.21±0.05	22±2	981±17	0	–	0.12±0.01	0.10±0.88	36±8
0716+714	UB	53±5	0.71±0.08	17±1	1.49±0.09	0.16±0.02	7±2	62±17	0.45±0.10	30±4	0.77±0.10	0.11±1.11	4±4
	UA1	1307±121	0	–	0.20±0.02	0.21±0.21	+25±9	1238±124	0	–	0.31±0.03	0.31±0.07	+34±3
0836+710	UA2	213±93	0.31±0.11	–138±6	0.21±0.02	0.98±1.47	–160±180	226±120	0.12±0.10	–138±39	0.32±0.10	0.76±1.14	–137±62
	UA3	61±66	0.66±0.20	–129±4	0.30±0.22	0.91±0.96	+32±48	84±7	0.73±0.09	–129±1	0.33±0.04	0.51±0.32	48±19
	UB	29±4	1.55±0.09	–139±1	0.48±0.13	0.79±0.40	+59±71	30±4	1.60±0.09	–139±1	0.65±0.15	0.57±0.22	+48±19
	UC	100±2	2.88±0.09	–144±1	0.69±0.03	0.68±0.04	+30±6	101±2	2.92±0.09	–144±1	0.67±0.04	0.67±0.03	+13±4
	UF	53±3	12.16±0.09	–148±1	2.76±0.17	0.46±0.05	–8±4	53±2	12.09±0.09	–147±1	2.58±0.14	0.38±0.03	–1±2
	UA	883±2	0	–	0.27±0.01	0.34±0.01	100±1	785±2	0	–	0.32±0.01	0.43±0.01	101±1
	UB <sup>a</sup>	29±6	1.12±0.07	–68±2	1.13±0.24	0.26±0.11	–80±6	48±2	1.68±0.06	–65±1	2.22±0.15	0.11±0.04	109±1
1039+811	UC <sup>a</sup>	23±4	2.38±0.11	–67±1	1.36±0.18	0.09±0.12	–92±4						
	UA	405±35	0	–	0.25±0.03	0.32±0.17	63±5	355±72	0	–	0.14±0.07	0.20±0.19	60±12
	UB1	157±38	0.33±0.06	233±2	0.19±0.07	0.17±0.15	69±17	172±78	0.34±0.06	239±3	0.29±0.12	0.84±0.41	31±102
1150+812	UB2	113±14	0.65±0.06	221±2	0.65±0.04	0.44±0.05	–15±5	78±29	0.74±0.09	218±3	0.48±0.14	0.17±0.50	23±12
	UC	102±5	1.97±0.06	170±1	2.15±0.76	0.23±0.25	–26±1	130±10	1.89±0.09	182±1	1.62±0.15	0.35±0.04	172±1
	UD	153±3	2.21±0.06	183±1	0.66±0.02	0.76±0.02	–6±3	158±14	2.31±0.06	178±1	0.90±0.02	0.62±0.04	–71±2
	UE	55±4	3.59±0.13	168±1	2.10±0.13	0.74±0.06	–59±10	28±4	4.23±0.20	162±1	3.11±0.46	0.26±0.05	–26±2
	UA	198±6	0	–	0.26±0.21	0.22±0.17	–17±15	218±8	0	–	0.42±0.27	0.19±0.15	–36±19
	UB	78±6	0.26±0.02	–48±3	0.43±0.23	0.11±0.10	–70±25	105±8	0.39±0.02	–48±2	0.31±0.17	0.09±0.07	–88±23
	UC1	12±1	1.11±0.04	–61±3	0.28±0.20	0.30±0.16	–169±35	16±1	1.28±0.05	–63±2	0.45±0.27	0.56±0.23	143±28
1749+701	UC2	15±2	1.42±0.04	–77±2	0.42±0.23	0.63±0.19	48±15						
	UD	31±2	2.25±0.02	–73±2	0.74±0.32	0.47±0.21	51±8	47±2	2.40±0.02	–70±1	0.66±0.30	0.43±0.17	71±14
	UE1	55±3	3.19±0.12	–57±1	3.09±0.16	0.42±0.15	–44±7						
	UE2							28±2	3.65±0.13	–54±2	2.40±0.22	0.21±0.14	87±11
	UA	1920±7	0	–	0.13±0.01	0.81±0.06	–47±15	1233±70	0	–	0.09±0.01	0.54±0.41	6±15
	UB1	494±6	0.28±0.06	–76±2	0.32±0.05	0.67±0.08	82±7	538±61	0.20±0.06	–72±5	0.36±0.04	0.56±0.07	86±8
	UB2	194±31	0.80±0.06	–77±1	0.45±0.06	0.55±0.08	126±4	225±51	0.70±0.09	–79±2	0.84±0.14	0.28±0.05	110±3
1803+784	UC	187±7	1.47±0.06	–90±1	0.57±0.02	0.63±0.03	66±3	198±32	1.44±0.06	–90±1	0.50±0.03	0.68±0.04	79±5
	UD	38±6	2.02±0.06	–93±1	0.92±0.07	0.60±0.09	164±6	47±9	1.82±0.38	–91±3	1.06±0.34	0.49±0.19	70±10
	UE	41±4	3.51±0.14	–92±1	3.18±0.27	0.39±0.05	102±4	70±5	3.52±0.17	–92±1	4.44±0.31	0.35±0.04	91±2
	UA	941±25	0.26±0.11	–20±6	0.20±0.10	0.26±0.13	–6±1	774±8	0.39±0.14	–16±1	0.52±0.01	0.11±0.03	–13±2
	UB1	656±27	0	–	0.23±0.01	0.16±0.08	–19±2	602±20	0	–	0.52±0.01	0.11±0.03	–14±1
1928+738	UB2	571±30	0.38±0.11	155±1	0.34±0.02	0.61±0.03	–28±1	660±13	0.32±0.14	143±1	0.38±0.09	0.27±0.02	–13±1
	UC	390±2	1.15±0.11	152±1	0.34±0.02	0.61±0.03	6±2	331±1	1.26±0.14	152±1	0.31±0.08	0.72±0.14	–38±3
	UD	184±3	2.50±0.11	162±1	0.91±0.02	0.52±0.02	19±2	184±6	2.55±0.14	158±1	0.57±0.04	0.44±0.04	–165±2
	UE	157±2	2.96±0.11	173±1	1.27±0.02	0.17±0.05	–14±2	181±2	3.07±0.14	173±1	1.22±0.12	0.31±0.01	–13±1
	UF	40±2	3.93±0.11	162±1	0.72±0.05	0.13±0.32	–46±9	63±3	3.82±0.14	163±1	1.38±0.10	0.39±0.05	–32±6
	UG	19±1	5.57±0.11	164±1	0.61±0.05	0.23±0.23	–79±13	11±2	5.26±0.14	168±2	1.59±0.45	0.17±0.16	21±7
	UI	76±3	11.46±0.11	167±1	2.60±0.10	0.65±0.05	–15±5	93±3	11.58±0.14	167±1	2.46±0.16	0.84±0.08	6±13
	UA1	283±12	0.29±0.05	–96±2	0.18±0.04	0.22±0.21	39±25	516±15	0.22±0.05	85±1	0.14±0.04	0.25±0.08	82±20
	UA2	223±26	0	–	0.20±0.02	0.12±0.12	93±8	278±14	0	–	0.14±0.08	0.17±0.09	–45±3
2007+777	UB1 <sup>a</sup>	146±21	0.32±0.05	–84±2	0.15±0.04	0.50±0.41	37±20	323±2	0.38±0.05	–82±1	0.21±0.03	0.61±0.02	100±2
	UB2 <sup>a</sup>	94±22	0.63±0.07	–86±1	0.62±0.11	0.65±0.12	107±10						
	UC	51±2	1.44±0.05	–88±1	0.34±0.17	0.59±0.08	–66±7	112±1	1.48±0.05	–89±1	0.67±0.01	0.53±0.01	87±1
	UF	38±1	6.13±0.05	–90±1	1.94±0.08	0.44±0.03	–53±2	25±1	6.34±0.07	–95±1	3.19±0.16	0.28±0.03	107±2

Note: For each source component, we list its flux density, separation and position angle relative to the component fixed at the origin ( $r = 0, \theta = 0$ ), major axis, axis ratio, and position angle of the major axis. The uncertainties given here have been estimated from the exploration of the parameter space ( $S, r, \theta, a, b/a$ , and  $\phi$ ), and from empirical considerations (e.g., the nominal errors of the component positions are in general smaller than  $10\mu$  as, but to be conservative we increased this figure up to a tenth of a beam width).

<sup>a</sup> This component is model fitted as double only in the first epoch. In the second epoch the model fit algorithm merged both components into a single one.

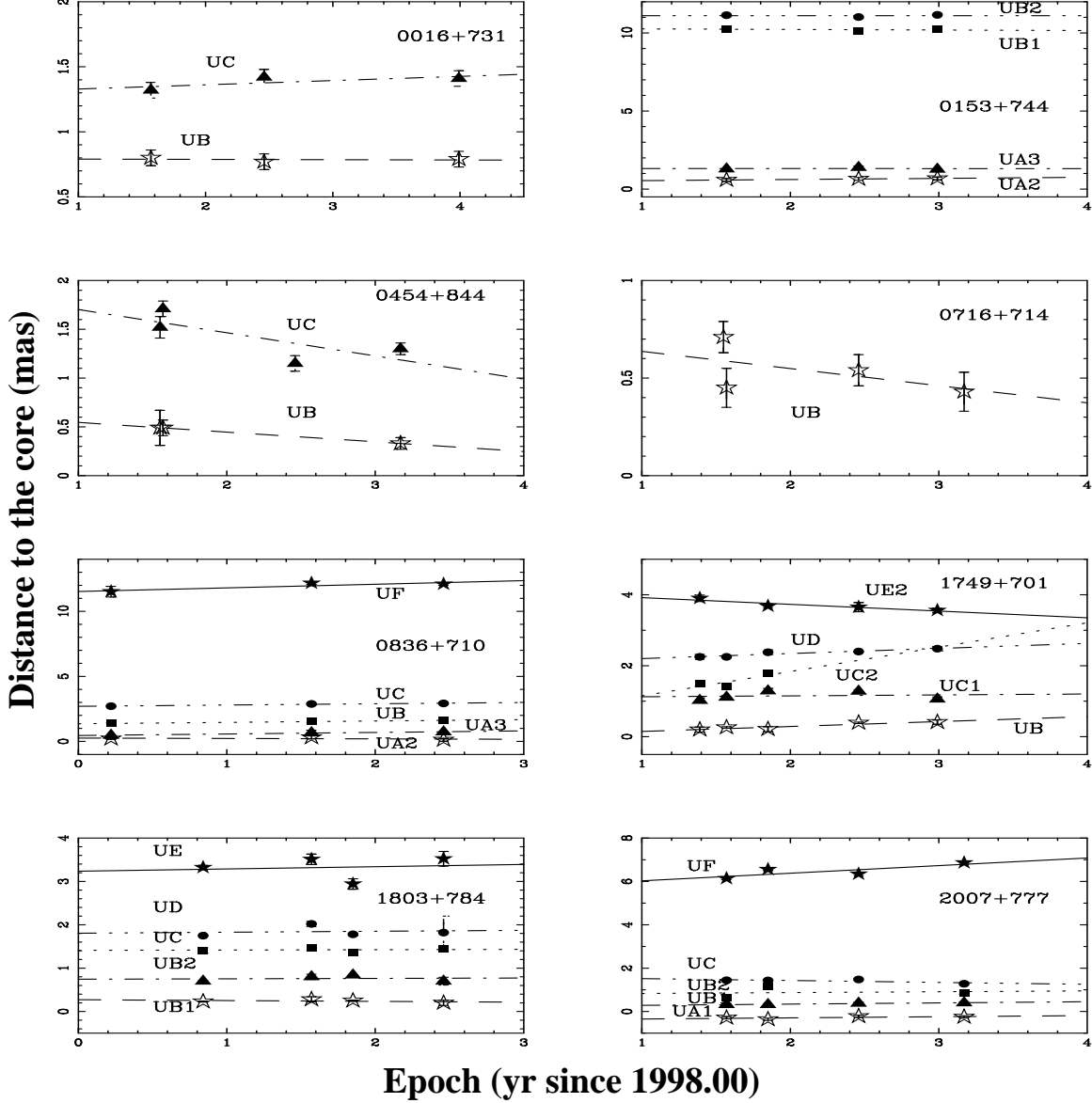


**Fig. 1.** Angular distance to the core vs. time elapsed since 1998.0. The plots show the change in angular separation with time of source features for which we have measured an angular velocity from observations at three or more epochs. The lines are linear fits to the data, the slope representing the proper motion,  $\mu$ , tabulated in Table 4.

Our model fit indicates a proper motion for UA2 of  $\mu = (71 \pm 6) \mu\text{as/yr}$  [ $\beta_{\text{app}} = (4.7 \text{ to } 0.4) h^{-1}$ ]. UA3, located at a radial distance of (1.3 to 1.4) mas at an angle  $90^\circ$ , does not show evidence for any proper motion. The extended, optically thin emission of the jet is characterized by two components, UB1 and UB2, that lie at an angular distance of  $(10.15 \pm 0.15)$  mas and  $(11.1 \pm 0.1)$  mas, respectively, and at an angle of  $\sim 150^\circ$ .

Since QSO 0153+744 did not show evidence of intraday variability (IDV) (A. Kraus, private communication), we assumed that the 8.4 GHz VLBA flux density of the source did not change between 1999.41 and 1999.57, and obtained a global spectral index  $\alpha = -0.79$ . We also ob-

tain  $\alpha \approx -0.01$  for component UA/XA (a perfect flat spectrum for the innermost regions of the core-jet structure). The sub-component XA1/UA1 has  $\alpha = 0.52$ , which supports our suggestion that this sub-component might be the core. We noticed that  $\alpha \approx -2.05$  for XB/UB, which corresponds to a synchrotron spectrum partially suppressed by an external medium. In this case, this would indicate that at a distance of  $\sim 60$  pc from the putative core the outer regions of the jet of QSO 0153+744 interact strongly with their surrounding medium. Finally, we failed to detect the jet components that in Paper I were found to form an arc between XA/UA and XB/UB, which results in upper limits of  $\alpha_{XC/UC} \lesssim -2.24$ ,  $\alpha_{XD/UD} \lesssim -3.09$ ,

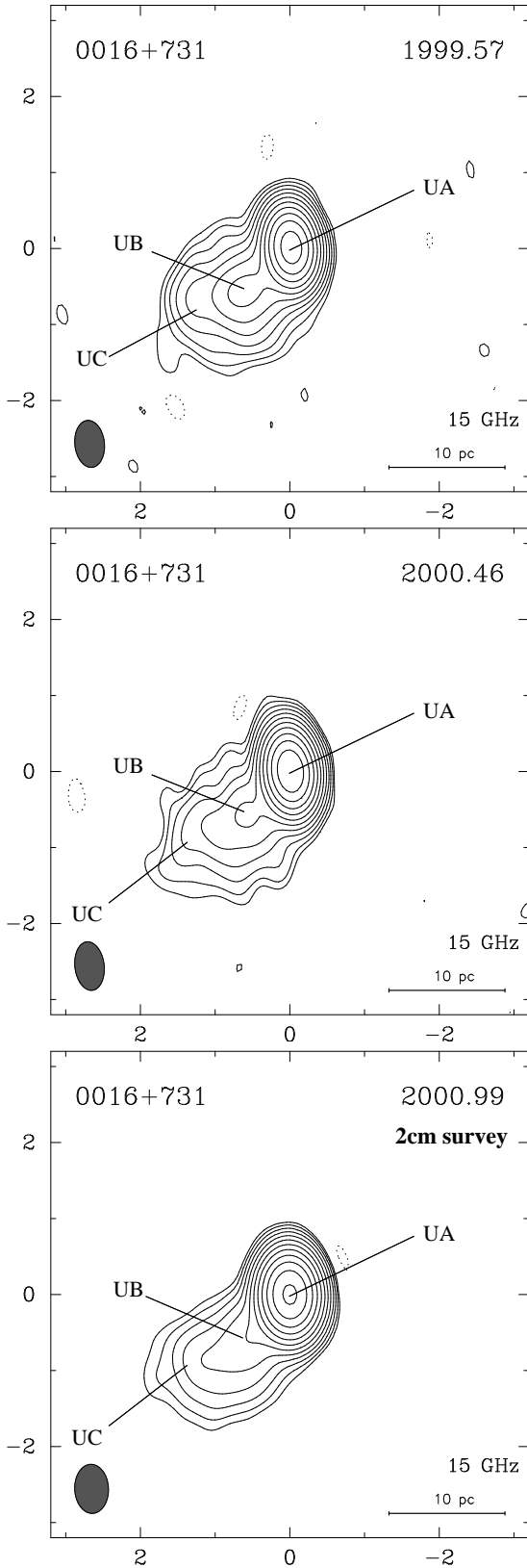


**Fig. 2.** VLBA images of QSO 0016+731 on 27 July 1999 (1999.57), 15 June 2000 (2000.46), and 28 December 2000 (2000.99). See Tables 1–3 for contour levels, beam sizes (bottom left in the maps), peak flux densities, and component parametrization. Axes are relative  $\alpha$  and  $\delta$  in mas.

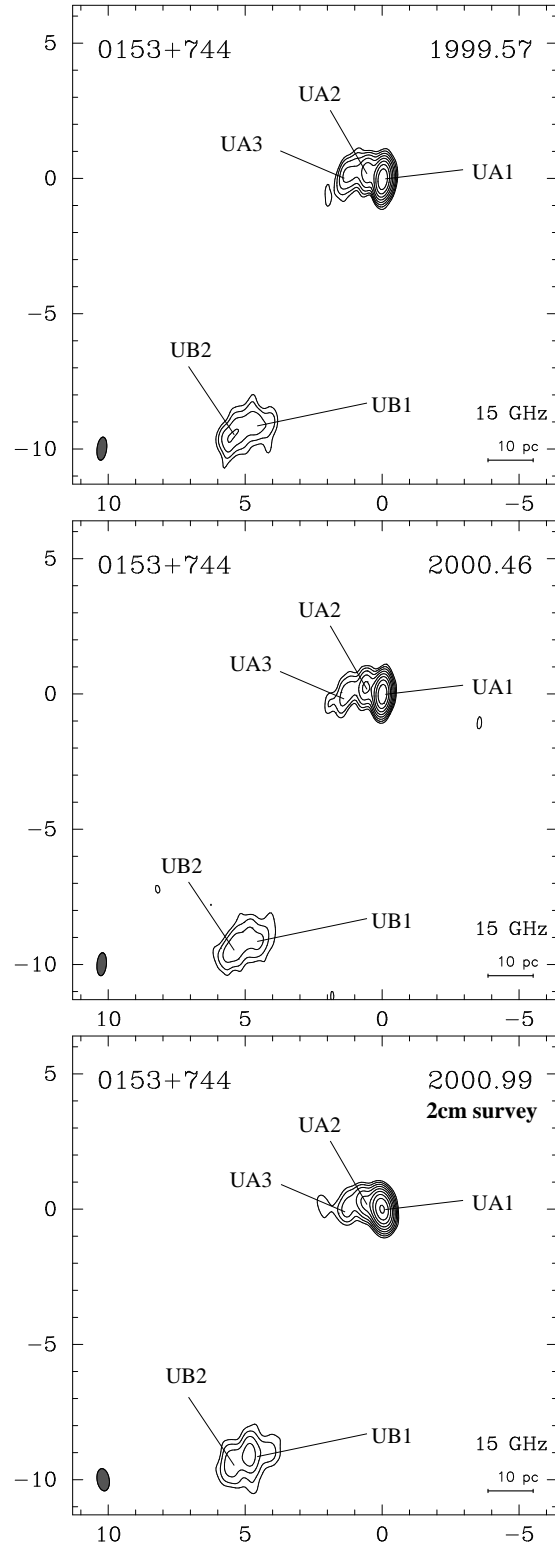


**Fig. 3.** VLBA images of QSO 0153+744 on 27 July 1999 (1999.57), 15 June 2000 (2000.46), and 28 December 2000 (2000.99). See Tables 1–3 for contour levels, beam sizes (bottom left in the maps), peak flux densities, and component parametrization. Axes are relative  $\alpha$  and  $\delta$  in mas.

**Table 3.** Map parameters and elliptical Gaussian component model parameters for selected sources of the complete S5 polar cap sample from the 2 cm Survey

Source	Comp.	$S$ [mJy]	$r$ [mas]	$\theta$	$a$ [mas]	$b/a$	$\phi$
<b>0016+731</b> — <i>Epoch 2000.99, (0.647×0.452, 2.4)<sup>a</sup>, 731<sup>b</sup>, 811<sup>c</sup>, 0.5<sup>d</sup></i>							
UA		742±1	0	—	0.09±0.01	0.30±0.08	-81±1
UB		35±6	0.79±0.06	140±1	0.55±0.05	0.88±0.08	178±28
UC		36±6	1.41±0.06	131±1	0.76±0.07	0.84±0.09	88±21
<b>0153+744</b> — <i>Epoch 2000.99, (0.833×0.446, 8.9), 188, 288, 0.7</i>							
UA1		190±1	0	—	0.13±0.01	0.16±15.0	74±8
UA2		28±2	0.68±0.08	69±1	0.31±0.05	0.20±0.25	-96±15
UA3		17±1	1.27±0.08	87±2	0.63±0.10	0.11±0.13	153±10
UB1		42±3	10.24±0.08	153±1	1.01±0.10	0.79±0.11	131±15
UB2		14±3	11.16±0.08	151±1	0.53±0.09	0.86±0.26	57±125
<b>0454+844</b> — <i>Epoch 1999.55, (0.687×0.492, -14.8), 126, 186, 0.6</i>							
UA		144±12	0	—	0.34±0.02	0.58±0.06	18±5
UB		24±13	0.49±0.18	134±7	0.78±0.29	0.20±0.17	-22±9
UC		18±3	1.52±0.11	168±2	1.34±0.24	0.47±0.10	19±7
<i>Epoch 2001.17, (0.641×0.411, 15.4), 187, 257, 0.7</i>							
UA		201±6	0	—	0.23±0.01	0.30±0.10	16±3
UB		39±5	0.33±0.06	138±2	0.23±0.21	0.30±0.27	75±12
UC		22±1	1.30±0.06	158±1	0.74±0.03	0.70±0.08	83±8
<b>0716+714</b> — <i>Epoch 1999.55, (0.849×0.551, 8.3), 1176, 1254, 0.6</i>							
UA		1174±8	0	—	0.14±0.01	0.37±0.03	34±3
UB		63±9	0.54±0.08	16±1	0.89±0.11	0.13±0.05	11±2
UC		13±1	1.85±0.09	9±1	1.08±0.33	0.66±0.35	157±16
UD		7±1	3.69±0.12	20±2	1.86±0.37	0.38±0.17	89±13
<i>Epoch 2001.17, (0.770×0.451, 31.9), 572, 643, 0.3</i>							
UA		549±33	0	—	0.12±0.05	0.27±0.06	28±4
UB		71±34	0.43±0.10	22±2	0.35±0.16	0.47±0.26	16±9
UC		15±2	1.94±0.09	19±1	1.27±0.16	0.38±0.05	8±4
UD		8±2	3.95±0.35	15±2	3.28±0.65	0.22±0.07	27±5
<b>0836+710</b> — <i>Epoch 1998.22, (0.681×0.442, -12.5), 1378, 2298, 1.0</i>							
UA1		1672±26	0	—	0.38±0.01	0.69±0.01	33±19
UA2		228±33	0.21±0.04	-84±2	0.21±0.03	0.63±0.26	-139±42
UA3		60±9	0.47±0.04	-114±2	0.34±0.21	0.35±1.0	69±13
UB		38±1	1.37±0.04	-135±1	0.39±0.26	0.84±0.93	174±19
UC		159±1	2.71±0.04	-141±1	0.69±0.01	0.81±0.01	19±2
UF		72±3	11.61±0.41	-147±1	3.17±0.14	0.41±0.03	2±5
<b>1749+701</b> — <i>Epoch 1999.39, (0.657×0.419, -12.6), 246, 415, 0.5</i>							
UA		196±3	0	—	0.15±0.01	0.22±0.13	-17±4
UB		95±3	0.20±0.07	-48±1	0.32±0.01	0.32±0.10	-63±2
UC1		28±1	1.02±0.07	-62±1	0.43±0.36	0.61±0.07	-84±7
UC2		22±1	1.49±0.07	-75±1	0.37±0.02	0.86±0.14	65±24
UD		30±1	2.25±0.07	-73±1	0.68±0.03	0.80±0.05	-25±6
UE1		26±2	2.80±0.08	-59±1	1.43±0.07	0.90±0.08	-1±10
UE2		22±3	3.90±0.09	-53±1	1.79±0.12	0.77±0.07	84±11
<i>Epoch 1999.85, (0.715×0.446, -25.9), 299, 446, 0.4</i>							
UA		229±4	0	—	0.10±0.02	0.24±0.13	-39±6
UB		103±4	0.21±0.07	-49±1	0.41±0.01	0.20±0.04	-54±2
UC1		25±1	1.29±0.07	-67±1	0.67±0.02	0.20±0.14	78±3
UC2		15±1	1.78±0.07	-77±1	0.83±0.06	0.38±0.06	120±4
UD		34±1	2.38±0.07	-70±1	0.75±0.02	0.66±0.04	15±4
UE1							
UE2		37±1	3.68±0.04	-53±1	1.86±0.04	0.84±0.04	154±8
<i>Epoch 2000.99, (0.640×0.441, 20.4), 271, 434, 0.5</i>							
UA		245±1	0	—	0.05±0.20	0.25±0.26	-8±17
UB		111±4	0.41±0.06	-51±1	0.43±0.01	0.31±0.03	-52±1
UC1		12±1	1.06±0.06	-69±1	0.61±0.05	0.93±0.51	-62±84
UC2							
UD		36±1	2.48±0.06	-71±1	0.78±0.02	0.93±0.04	56±25
UE1							
UE2		34±2	3.56±0.06	-53±1	3.03±0.13	0.74±0.06	8±9

$\alpha_{XE/UE} \lesssim -3.09$ , at the  $3\sigma$  level. The spectral behaviour displayed by component XB/UB, as well as the non-detection of any significant motion, is typical of a sta-

**Table 3.** *Continued*

Source	Comp.	$S$ [mJy]	$r$ [mas]	$\theta$	$a$ [mas]	$b/a$	$\phi$
<b>1803+784</b> — <i>Epoch 1998.84, (0.731×0.425, -8.8), 1498, 2291, 0.9</i>							
UA		1310±46	0	—	0.12±0.01	0.86±0.03	-74±36
UB1		452±43	0.23±0.01	-88±1	0.28±0.01	0.75±0.29	76±39
UB2		157±4	0.70±0.01	-80±1	0.81±0.28	0.46±0.47	102±55
UC		193±3	1.41±0.01	-93±1	0.33±0.35	0.79±0.02	17±3
UD		109±3	1.75±0.01	-99±1	0.59±0.28	0.70±0.14	165±3
UE		52±2	3.32±0.05	-93±1	2.93±0.11	0.43±0.03	106±25
<i>Epoch 1999.85, (0.660×0.465, -27.9), 1777, 2518, 1.1</i>							
UA		1531±27	0	—	0.10±0.01	0.74±0.08	-63±15
UB1		494±25	0.25±0.01	-80±1	0.28±0.17	0.77±0.05	119±17
UB2		145±4	0.84±0.01	-76±1	0.48±0.02	0.45±0.03	131±4
UC		201±5	1.37±0.01	-88±1	0.52±0.01	0.38±0.10	64±13
UD		50±3	1.78±0.03	-98±1	0.75±0.48	0.52±0.41	127±23
UE		44±1	2.94±0.04	-96±1	1.67±0.95	0.70±0.52	107±6
<b>2007+777</b> — <i>Epoch 1999.85, (0.653×0.447, 0.6), 428, 929, 0.4</i>							
UA1		413±1	0.36±0.01	93±1	0.17±0.01	0.28±0.03	91±25
UA2		163±1	0	—	0.20±0.01	0.26±0.07	90±23
UB1		230±1	0.32±0.01	-86±1	0.13±0.01	0.75±0.24	65±18
UB2		75±2	1.14±0.01	-91±1	0.52±0.23	0.82±0.01	152±3
UC		24±1	1.43±0.01	-88±1	0.43±0.17	0.38±0.10	-81±3
UF		28±1	6.55±0.02	-94±1	1.30±0.05	0.73±0.06	83±7
<i>Epoch 2001.17, (0.617×0.421, -0.9), 393, 948, 0.4</i>							
UA1		330±7	0.25±0.01	87±1	0.17±0.01	0.22±0.15	85±1
UA2		189±4	0	—	0.38±0.01	0.24±0.03	90±1
UB1		213±3	0.40±0.01	-87±1	0.22±0.01	0.37±0.05	104±2
UB2		115±1	0.87±0.01	-76±1	0.52±0.01	0.38±0.03	104±1
UC		77±1	1.28±0.01	-96±1	0.46±0.01	0.54±0.03	-79±2
UE		7±1	5.08±0.03	-106±1	0.82±0.08	0.31±0.29	112±7
UF		15±1	6.86±0.06	-95±1	2.08±0.15	0.29±0.06	71±3

Note: For each source component, we list its flux density, separation and position angle relative to the component fixed at the origin ( $r = 0, \theta = 0$ ), major axis, axis ratio, and position angle of the major axis. The uncertainties given here have been estimated from the exploration of the parameter space ( $S, r, \theta, a, b/a$ , and  $\phi$ ), and from empirical considerations (e.g., the nominal errors of the component positions are in general smaller than  $10\mu\text{as}$ , but to be conservative we increased this figure up to a tenth of a beam width).

- <sup>a</sup> The restoring beam is an elliptical Gaussian with FWHM axes  $a \times b$  [mas]. For each source, the position angle (P.A.) stands for the direction of the major axis, measured north through east.  
<sup>b</sup>  $S_{\text{peak}}$ : brightness peak [mJy/beam].  
<sup>c</sup>  $S_{\text{tot}}$ : total flux density recovered in the hybrid mapping process [mJy].  
<sup>d</sup> rms: root-mean-square noise in the image [mJy]. Contours in the maps of the figures shown in Sects. 3.1 to 3.13 are the tabulated rms values times  $(-3, 3, 3\sqrt{3}, \dots)$ .

tionary region of the jet, thus confirming the finding by Hummel et al. (1997).

### 3.3. QSO 0212+735

QSO 0212+735 (Fig. 4,  $z=2.367$ ) is the most distant source of the complete S5 polar cap sample. Our 15.4 GHz VLBA maps show a jet-like structure extending eastwards up to 14 mas ( $\approx 85 h^{-1}$  pc, the longest jet in the sample). The total flux density of QSO 0212+735 remained virtually constant between our two observing epochs. Our maps and model fit show two distinct regions in QSO 0212+735: the inner core-jet region, formed by components UA, UB1 and UB2; and the extended, weaker region of the jet, composed of UC, UD, and UG.

**Table 4.** Proper motions<sup>†</sup> in the S5 polar cap sample

Source	Comp.	$\mu$ [ $\mu$ as/yr]	$\beta_{\text{app}}$ [ $v_{\text{app}}/c$ ]
0016 + 731	UC	$32 \pm 31$	$1.9 \pm 1.8$
0153 + 744	UA2	$71 \pm 6$	$4.7 \pm 0.4$
0454 + 844	UB	$-100 \pm 3$	$-5.1 \pm 0.2$
	UC	$-217 \pm 140$	$-11.0 \pm 7.4$
0716 + 714	UB	$-105 \pm 100$	$-1.6 \pm 1.5$
0836 + 710	UA2	$-13 \pm 6$	$-0.8 \pm 0.4$
	UA3	$118 \pm 7$	$7.6 \pm 0.5$
	UB	$110 \pm 16$	$7.1 \pm 1.0$
1749 + 701	UC	$101 \pm 16$	$6.5 \pm 1.0$
	UB	$141 \pm 25$	$5.1 \pm 0.9$
	UC2	$732 \pm 603$	$26.5 \pm 21.8$
1803 + 784	UD	$161 \pm 19$	$5.8 \pm 0.7$
	UE2	$-150 \pm 62$	$-5.4 \pm 2.2$
	UB1	$17 \pm 16$	$0.6 \pm 0.5$
2007 + 777	UB2	$133 \pm 24$	$4.4 \pm 0.8$
	UA1	$52 \pm 48$	$1.0 \pm 1.0$
2007 + 777	UB1	$56 \pm 11$	$1.1 \pm 0.2$
	UC	$-88 \pm 61$	$-1.8 \pm 1.2$
	UF	$350 \pm 203$	$7.0 \pm 4.0$

<sup>†</sup>Proper motions are listed for components observed at three or more epochs, whose least-squares fit showed a motion larger than  $1\sigma$ , which is the quoted uncertainty. See details in the main text and Fig. 3.1.

The value of  $Q$  (UA emission to extended emission), increased from 0.8 to 1.0 between 1999.57 and 2000.46. This is one of the lowest values of  $Q$  found in the sample, indicating that the extended emission contributes about the same amount as the emission from the core. This is so because component UB (which we suggest is at the base of the jet, and does not belong to the core region) is as strong as the core itself. (If for  $Q$  we take the emission from UA+UB to the extended emission, we obtain 17.5 and 15.2, in 1999.57 and 2000.46, respectively, and we would say the source is “core”-dominated.) The flux density of QSO 0212+735 puts it among the three brightest sources of the sample and, given its redshift, it is the most powerful source with a monochromatic luminosity of  $L_{15\text{ GHz}} = (9.2 \text{ to } 9.3) \times 10^{39} \text{ W}$ .

The flux density variations in each individual component of the innermost and outermost regions are marginally consistent ( $\sim 2\sigma$ ), with no change between the first and second epochs. The innermost region is the one that shows the most interesting features: component UA, the brightest component at both epochs and probably the core, lies at a distance of 0.6 mas ( $3.6 h^{-1} \text{ pc}$ ) from the origin, at an angle of  $\sim -47^\circ$ . Component UB1 is at the origin, while component UB2 is at a distance  $r \approx 0.26$  mas at angle  $\approx 90^\circ$ . The remaining components, UC, UD, and

UG, lie at distances of  $\approx 0.9$  mas, 2.5 mas, and 13.8 mas ( $\approx 83 h^{-1} \text{ pc}$ ) respectively, and within an angle of  $90^\circ$  to  $100^\circ$  at both epochs. Our model fit for QSO 0212+735 gives no evidence for any significant proper motion either in the innermost or the outermost region. (We note that QSO 0212+735 is one of only three sources in the sample for which the brightest component is not at the origin of the coordinates; see Table 1.)

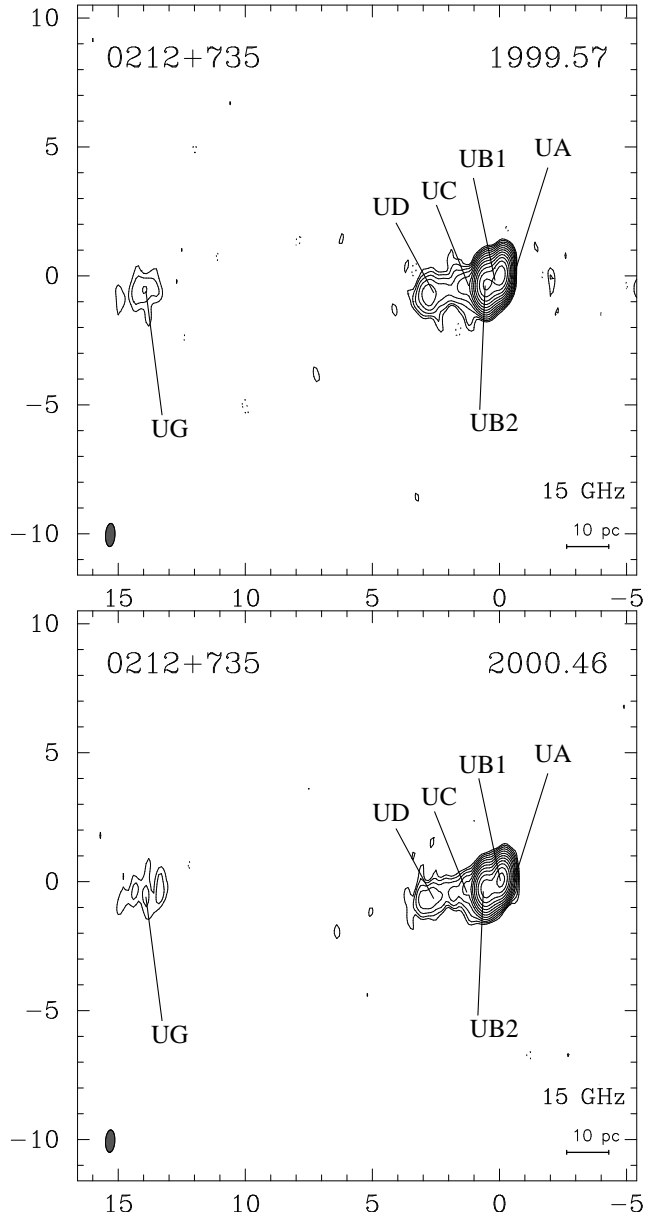


**Fig. 4.** VLBA images of QSO 0212+735, from observations on 27 July 1999 (1999.57) and 15 June 2000 (2000.46). Axes are relative  $\alpha$  and  $\delta$  in mas. See Table 1 for contour levels, synthesized beam size (bottom left in the figure), and peak flux densities. See Table 2 for component parametrization.



Assuming that the 8.4 GHz flux density of the source did not change between 1999.41 and 1999.57, we obtain a global value of  $\alpha = -0.07$ . A detailed comparison of our model fit at 15.4 GHz for the first epoch with the model fit made at 8.4 GHz for the second epoch (see Paper I), gives the following results. The position of component XA nicely corresponds to that of UA. The inferred spectral index is then  $\alpha=0.78$ , a rather inverted spectrum, as we would expect if UA/XA were the core. Component XB is very likely a blend of two components (UB1 and UB2), which yields  $\alpha_{\text{UB/XB}} = -0.45$ . The positions at 8.4 GHz and 15.4 GHz for the remaining components are the same within the uncertainties. For those components, we find a progressive steepening of the spectral index with distance from the jet. Namely,  $\alpha_{\text{UC/XC}} = -0.49$ ,  $\alpha_{\text{UD/XD}} = -1.00$ , and  $\alpha_{\text{UG/XG}} = -1.76$ . The position of component UG/XG has remained remarkably stable, both in the X- and U-band between 1997.93 and 2000.46, at a nominal position of 13.8 mas at angle  $93^\circ$ . Most likely, component UG/XG is a stationary region of the source. We do not see emission from components UE+UF (clearly detected at 8.4 GHz as XE+XF; see Paper I) above  $3\sigma$ , which implies a very steep spectrum for those components.

### 3.4. BL 0454+844

BL 0454+844 is, at  $z \gtrsim 1.340$  (Stoche & Rector 1997), the most distant BL Lacertae source of our sample with known redshift. Its monochromatic luminosity is  $L_{15 \text{ GHz}} \approx (1.2 \text{ to } 2.6) \times 10^{38} \text{ W}$  (note that the previously accepted redshift for BL 0454+844,  $z = 0.112$ , implying a lower intrinsic luminosity by a factor of 200, which makes BL 0454+844 the least powerful radio source of the sample). BL 0454+844 shows, together with BL 0716+714, the least structure of all the sources of the complete sample, as seen at 15.4 GHz (Fig. 5). Indeed, there is no emission above  $3\sigma$  outside the inner 2 mas ( $13.2 h^{-1} \text{ pc}$ ) away from component UA. Our VLBA observations showed a significant variation in the flux density of BL 0454+844 between 1999.55 and 1999.57, decreasing from 186 mJy down to 120 mJy (35% change). It then started to slowly increase up to 131 mJy in 2000.46 (9% change), after which the source almost doubled its total flux density in less than nine months (257 mJy in 2001.17). We fitted each observing epoch, except epoch 2000.46, with a three-component model (see Table 2), which seems a reasonable model fit of the radio source. We find the following values for the ratio  $Q$  (value, epoch: 3.43, 1999.55; 3.44, 1999.57; 6.37, 2000.46; 3.59, 2000.99). Those values seem to confirm the dominance of the core emission. Note that  $Q$  is significantly larger in 2000.46 than at the other epochs, while the map for this epoch does not show significant differences with, e.g., the map in 1999.57. This enhanced value of  $Q$  in 2000.46 must be taken with caution, as the somewhat noisier data for this

epoch resulted in a poorer model fit of the source structure.

At all epochs, most of the emission comes from component UA, likely to be the core, which contributes  $\approx 78\%$  of the total emission (except in 2000.46, where it amounts to  $\approx 92\%$ ; but see the caveat above). The spectral index for UA/XA is, assuming the 8.4 GHz did not change significantly between 1999.41 and 1999.55,  $\alpha_{\text{UA/XA}}=0.06$ , as expected for a core component. Component UB belongs to the innermost regions of BL 0454+844, lying at a distance of (0.3 to 0.5) mas from component UA, at an angle of  $140^\circ$ . Component UC traces the jet region of BL 0454+844. It probably consists of two or more sub-components, judging by the fact that the radial distances span a huge range (1.2 mas to 1.7 mas) in less than 20 months. Our model fit indicates a backwards proper motion for both components UB ( $\mu = (-100 \pm 3) \mu\text{as/yr}$ ;  $\beta_{\text{app}} = (-5.1 \pm 0.2) h^{-1}$ ), and UC ( $\mu = (-217 \pm 140) \mu\text{as/yr}$ ;  $\beta_{\text{app}} = (-11.0 \pm 7.4) h^{-1}$ ). However, the morphological structure of this source is so complex that those results must be taken with caution.

### 3.5. QSO 0615+820

Our VLBA maps of QSO 0615+820 (Fig. 6,  $z=0.710$ ) show a complex, albeit compact structure at both epochs, with a maximum extension  $\lesssim 2.5 \text{ mas}$  ( $=15.4 h^{-1} \text{ pc}$ ). The 15.4 GHz total flux density of the source slightly decreased between 1999.57 and 2000.46, from 434 mJy down to 410 mJy (6% change), with a monochromatic luminosity of  $L_{15 \text{ GHz}}=(1.0 \text{ to } 1.2) \times 10^{38} \text{ W}$ . Assuming that the 8.4 GHz flux density of the source did not change between 1999.41 and 1999.57, we obtain  $\alpha = -0.26$ , a moderately steep to flat spectrum for the milliarcsecond structure of the source.

We fitted reasonably well the milliarcsecond radio structure of QSO 0615+820 using three components (Table 2) within the inner 0.8 mas ( $5 h^{-1} \text{ pc}$ ). It might well be that components UA2 and UA3 consist, in turn, of two sub-components each, as the maps seem to hint, but this fact is not supported by the model fit at this stage. The coordinates of components UA1, UA2, and UA3 in 1999.57 are so close to those obtained in Paper I at 8.4 GHz (components XA1, XA2, and XA3 in 1999.41), that their physical association is very likely to be real. The ratio,  $Q$ , of the core (UA1) to the extended emission increased steadily with time (value, epoch: 0.88, 1999.55; 1.04, 1999.57; 1.44, 2000.46).

This object is, given the intriguing (and underlying) substructure of its components, worth being studied in detail. In particular, the core position is highly uncertain, and might not correspond to the position of UA1.

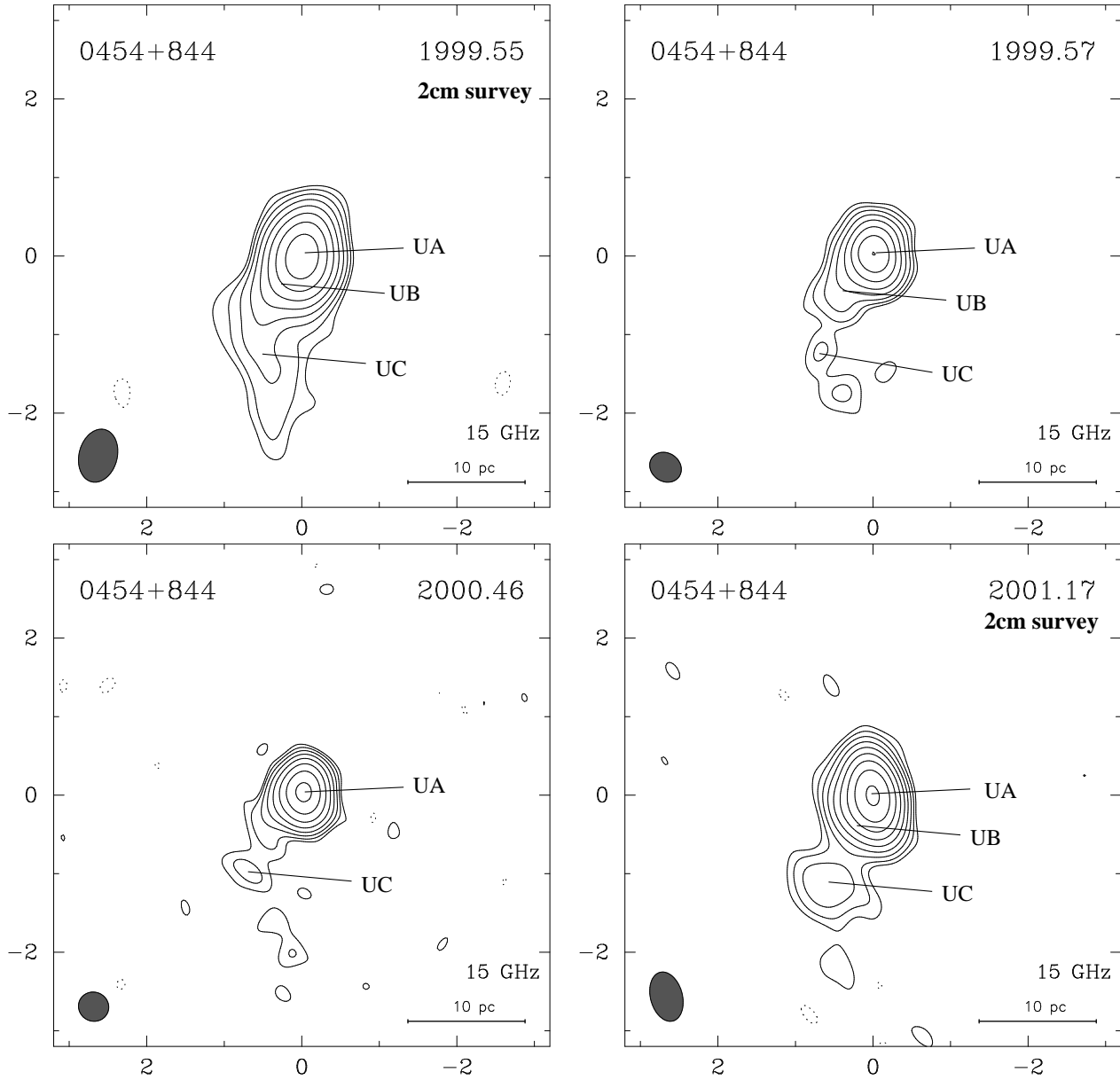


**Fig. 5.** VLBA images of BL 0454+844 from observations on 19 July 1999 (1999.55), 27 July 1999 (1999.57), 15 June 2000 (2000.46), and 4 March 2001 (2001.17). See Tables 1–3 for contour levels, beam sizes (bottom left in the maps), peak flux densities, and component parametrization. Axes are relative  $\alpha$  and  $\delta$  in mas.

### 3.6. BL 0716+714

BL 0716+714 is the only radio source of the sample whose redshift is unknown, though the absence of any host galaxy seems to rule out distances  $z \lesssim 0.25$  even for a low luminosity object (Wagner et al. 1996). The source displays intra-day variability (Quirrenbach et al. 1991; Wagner et al. 1996). The total flux density of BL 0716+714 at 15.4 GHz halved its value between 1999.55 and 2001.17 (19 months), decreasing from 1254 mJy down to 643 mJy, in accordance with the fact that BL 0716+714 is also a long-term variable. (At 8.4 GHz, the source displayed an op-

posite, increasing trend between 1997.93 and 1999.41, its flux growing by a factor 2.6, from 377 mJy up to 990 mJy in less than 18 months [see Paper I]). At a redshift of 0.25, the monochromatic luminosity of BL 0716+714 is  $L_{15\text{ GHz}} \approx (1.8 \text{ to } 3.4) \times 10^{37} \text{ W}$ , a low-to-intermediate value for a BL Lac object.

The 15.4 GHz VLBA maps (Fig. 7) show a core-jet structure that extends northwards up to 4 mas. The appearance of the source at all epochs is very similar, and rather featureless but for the last epoch. Our observations at 8.4 GHz made in 1999.41 resemble a scaled-up version of the 15.4 GHz ones in 1999.57. We modeled the 15.4 GHz

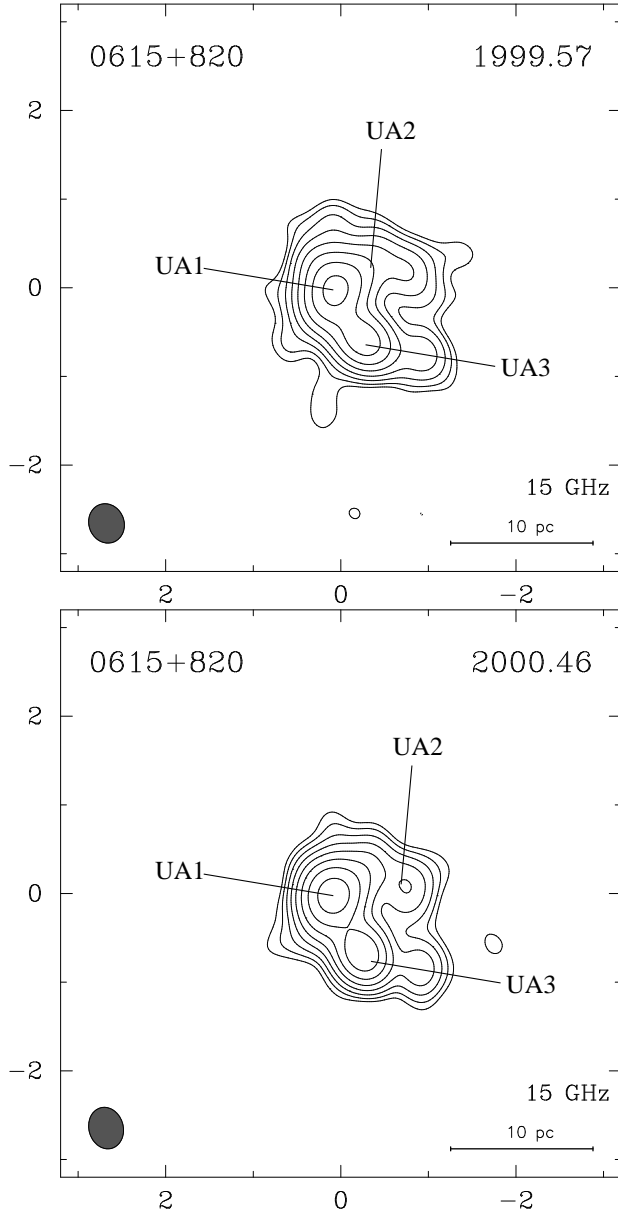


**Fig. 6.** VLBA images of QSO 0615+820 from observations on 27 July 1999 (1999.57) and 15 June 2000 (2000.46). Axes are relative  $\alpha$  and  $\delta$  in mas. See Table 1 for contour levels, synthesized beam sizes (bottom left in the maps), and peak flux densities. See Table 2 for component parametrization.

radio structure of BL 0716+714 in 1999.57 and 2000.46 with two components (see Table 2), instead of three, as we did for our 8.4 GHz observations (Paper I). Nonetheless, we had to use up to four components to model the source radio emission seen in 1999.55 and 2001.17, the two extra components being needed to account for the extended radio emission of the jet.

Component UA, the brightest one, is at the origin and contributes 85% to 96% of the total VLBA emission at all epochs. Its flux density evolves in almost exactly the

same way as the total flux of the source (the core activity drives the whole behaviour of the source). The ratios of the core (UA) to the extended emission were the following: (value, epoch: 14.7, 1999.55; 21.6, 1999.57; 14.0, 2000.46; 5.8, 2001.17). Those values make of BL 0716+714 one of the most compact and core dominated sources of the sample. The relatively low value of  $Q$  in 2001.17 is chiefly due to the decreasing flux density of the core (see the model fits in Table 3). Component UB probably lies close to the jet base. It contributes 5% to 11% of the total 15.4 GHz VLBA flux. The model fit algorithm gave significantly different values for the position of this component at each epoch (see Table 2). This could be an indication that motions could be taking place in this engine. Alternatively, it could be that UB is in fact composed of several sub-components. Unfortunately, neither the 8.4 GHz nor the 15.4 GHz VLBA observations have resolved the innermost structure of BL 0716+714. Our 43 GHz observations might yield enough resolution to say whether changes in its flux density are due to the emergence of components along the core-jet structure. The remaining 2% to 3% of the 15.4 GHz flux comes from components UC and UD, which are not well modeled in 1999.57 and 2000.46.

Our model fit for the source shows an inward proper motion for component UB (see Table 4), but only at the  $1\sigma$  level. Bach et al. (2003) have reanalysed multi-frequency VLBI data obtained between 1993 and 2001, and found that the source components display moderate superluminal motions ( $0.3 \text{ mas yr}^{-1}$ ;  $\beta_{\text{app}}=4.6 h^{-1}$ ) from the inner 3 mas of the jet, up to  $0.8 \text{ mas yr}^{-1}$  ( $\beta_{\text{app}}=12.3 h^{-1}$ ) for the outer regions of the jet.

Since BL 0716+714 is an intra-day variable, the assumption that the 15.4 GHz flux density of the source did not change between 1999.41 and 1999.55 is not well based. Yet, if we assume the flux density did not change we obtain  $\alpha_{UA/XA}=0.38$ , an inverted spectrum for the innermost structure of the source, in agreement with expectation if component UA/XA is the core.

### 3.7. QSO 0836+710 (4C 71.07)

The 15.4 GHz VLBA maps of QSO 0836+710 (Fig. 8;  $z=2.218$ , Véron-Cetty & Véron [2003]) show at all three epochs a rather complex, one-sided core-jet structure at P.A.  $\approx -(140^\circ \text{ to } 150^\circ)$ . We detected emission up to 12 mas ( $74 h^{-1} \text{ pc}$ ) away from the core. The source radio emission is well represented by six components, five of them within the inner 3 mas ( $10 h^{-1} \text{ pc}$ ) of the core, and one at a distance of 12 mas.

The 15.4 GHz total flux density of QSO 0836+710 varied significantly between 1998.22 and 1999.57, decreasing by 23%, from 2298 mJy down to 1766 mJy at a monthly rate of 1.4%. It continued to decrease until 2000.46 (down to 1728 mJy, a further 2% decrease at the much slower rate of 0.2% per month). QSO 0836+710 is the fourth bright-

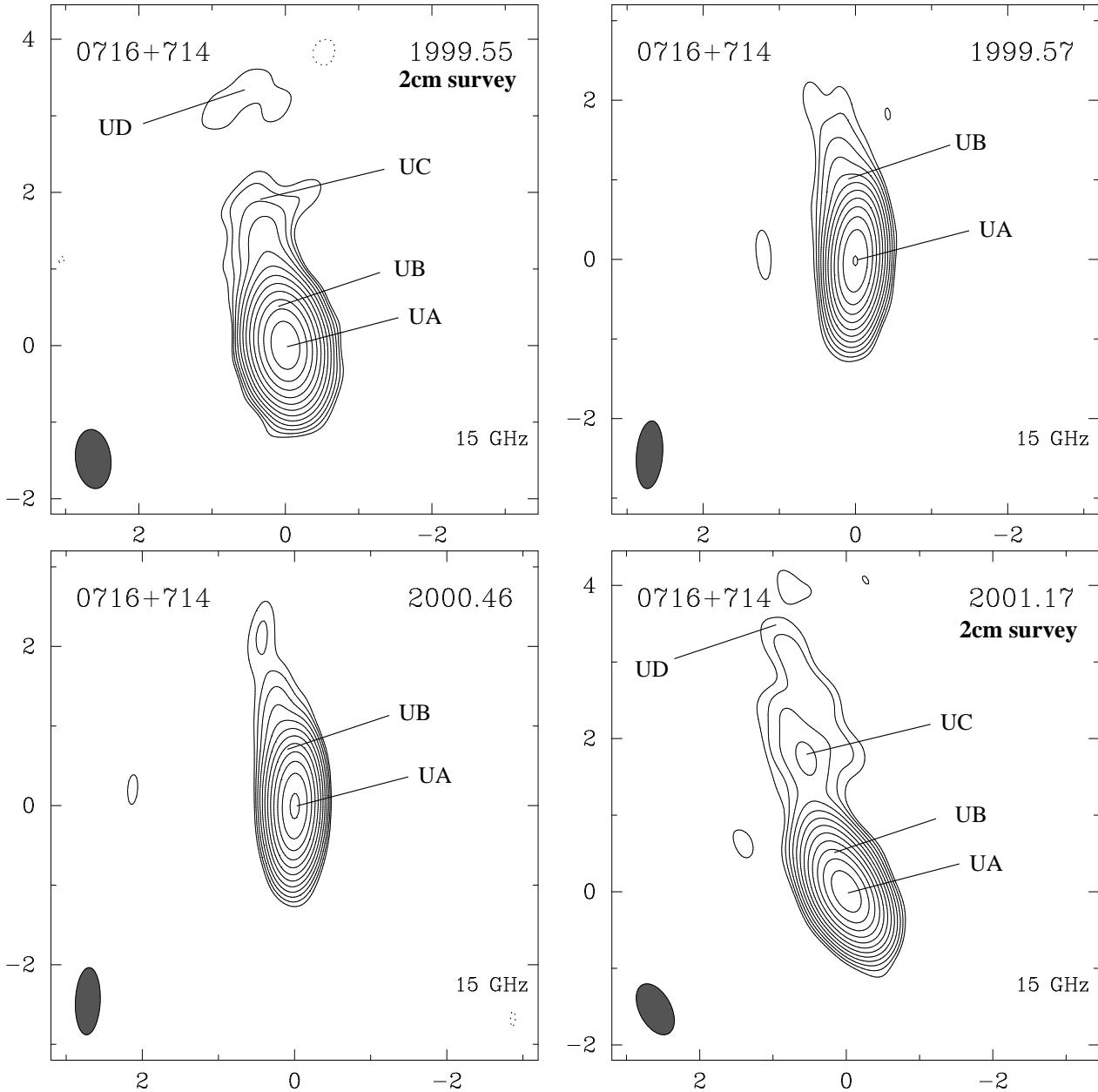


**Fig. 7.** VLBA images of BL 0716+714 from observations on 19 July 1999 (1999.55), 27 July 1999 (1999.57), 15 June 2000 (2000.46), and 4 March 2001 (2001.17). See Tables 1–3 for contour levels, beam sizes (bottom left in the maps), peak flux densities, and component parametrization. Axes are relative  $\alpha$  and  $\delta$  in mas.

est object of the complete sample, yet it is the second most powerful emitter with  $L_{15\text{ GHz}} \approx (5.5 \text{ to } 7.3) \times 10^{39} \text{ W}$ . The flux density trend of the brightest component, UA1 (likely the core), seems to follow that of the overall source. The values of the core-to-extended emission,  $Q$ , were 2.7 (1998.22), 2.9 (1999.57), and 2.5 (2000.46), indicative of a relatively compact, core-dominated source. The flux density of component UA2 remained very stable with time, at the 220 mJy level (10% to 13% of the total flux density), but its radial distance is uncertain. Component UA3, at a 30 mJy level, contributes about 2% of the

total flux density. Provided the 8.4 GHz flux density of the (XA+XB) region did not change significantly between 1999.41 and 1999.57, we obtain  $\alpha_{\text{UA}/(\text{XA}+\text{XB})} = 0.27$ . This value indicates an inverted spectrum for the innermost region source, and suggests that UA is likely to be the core (namely, UA1, which dominates the emission of the region). UB, at a distance of  $(1.5 \pm 0.1) \text{ mas}$  ( $\approx 5 h^{-1} \text{ pc}$ ) at an angle of  $140^\circ$  sets the transition from the core region to the extended emission of the jet. Its contribution remained constant at the 2% level at all epochs. Similarly,

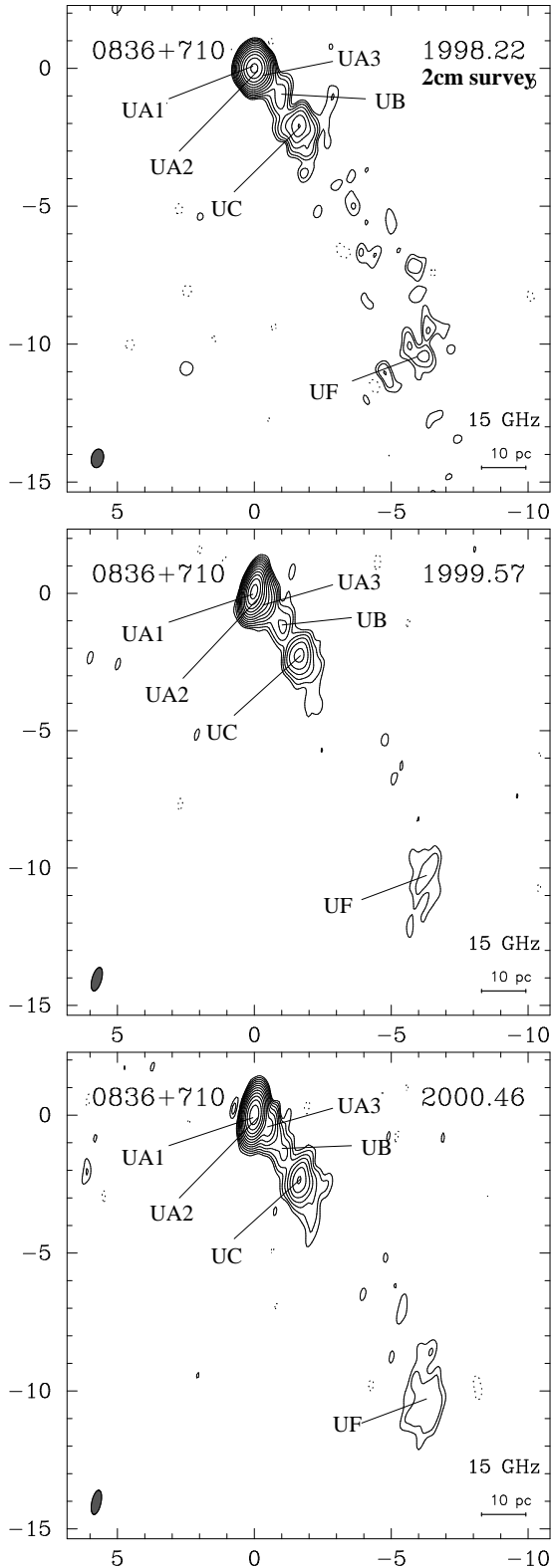


**Fig. 8.** VLBA images of QSO 0836+710 from observations on 20 March 1998 (1998.22), 27 July 1999 (1999.57), and 15 June 2000 (2000.46). See Tables 1–3 for contour levels, beam sizes (bottom left in the maps), peak flux densities, and component parametrization. Axes are relative  $\alpha$  and  $\delta$  in mas.

the spectral indices of components UC/XC and UF/XF are  $\alpha_{UC/XC} = -1.21$  and  $\alpha_{UF/XF} = -1.36$ , respectively.

Compared to our 8.4 GHz VLBA maps, we now have a clearer view of the innermost regions of the source. In particular, we are able to disentangle the fine structure of XA into three sub-components: UA1, UA2, and UA3. Component XB in Paper I is likely the result of a blending of several subcomponents at 15.4 GHz, most probably UA3 and UB.

Our model fit suggests the existence of superluminal motions for components UA3, UB, and UC ( $\beta_{app} \approx 7 h^{-1}$ ; see Table 4). We identified components UC and UF with XC and XF, respectively (Paper I). The positions of UF are consistent with no superluminal motion, which suggests that it is a stationary feature in the jet. UF shows an optically thin spectrum. We detected no emission from components XD or XE above our  $3\sigma$  level of 2.4 mJy in 1999.57. Our non-detection implies an upper limit for their synchrotron spectra of  $\alpha \lesssim -1.34$  and  $\alpha \lesssim -2.07$ . The disappearance of the jet beyond component UC might well be due to the prominent curvature displayed at 5 GHz, as shown in exquisite detail with VSOP (Lobanov et al. 1998), and to a lesser extent in our 8.4 GHz VLBA images (Paper I).

The ejection of a new component at mas scales reported by Otterbein et al. (1998) at epoch 1992.65, with an apparent superluminal motion of  $\mu = (0.26 \pm 0.03) \text{ mas/yr}$  has been directly related to gamma-, X-ray, and optical activity observed in February 1992 by these authors (Otterbein et al. 1998). The intense radio activity shown in the inner 1.5 mas from our 15.4 GHz VLBA observations seems to suggest the ejection of at least one new component.

### 3.8. QSO 1039+811

Our VLBA maps of QSO 1039+811 (Fig. 9,  $z=1.264$ ) show a relatively simple, one-sided core-jet structure at an angle of  $-70^\circ$  at pc-scales. The 15.4 GHz jet extends up to 3 mas ( $20 h^{-1} \text{ pc}$ ) from the core, a much less extended jet than seen at 8.4 GHz (8 mas long; see Paper I). The emission is heavily concentrated within the core region (UA), which contributes more than 94% of the total VLBA flux density at 15.4 GHz at both epochs. The remaining 6% comes from the weak, relatively extended jet. Correspondingly, the ratio of the core-to-jet emission,  $Q$ , was as large as 21 in 1999.57, and 19 in 2000.46, making of QSO 1039+811 the most compact, core-dominated QSO of the complete sample. The jet shows some substructure, which we are able to model as two components in the first epoch (components UB1 and UB2, 50 mJy). These components are model fitted as just one blended component at the second epoch, having almost the same flux density of UB1+UB2. Although our maps show that the jet morphology seems to have experienced dramatic changes between 1999.57 and

2000.46, its interpretation should be taken with caution. In particular, our second epoch is noisier than the first one, thus resulting in a lower confidence of the position of the features inside the jet.

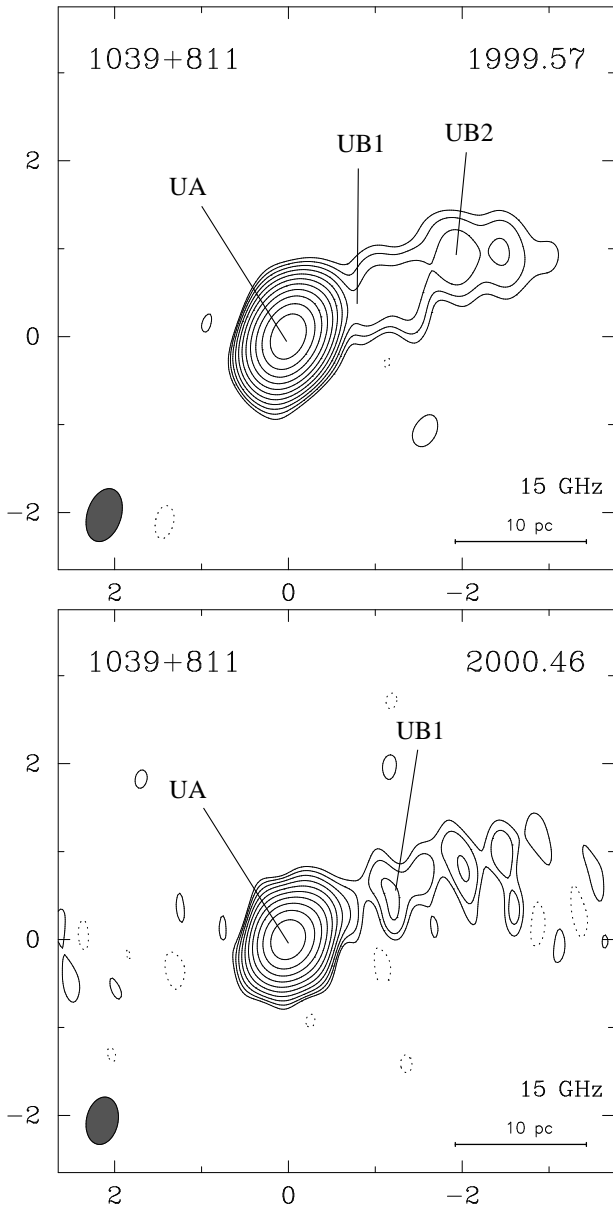


**Fig. 9.** VLBA images of QSO 1039+811 from observations on 27 July 1999 (1999.57) and 15 June 2000 (2000.46). Axes are relative  $\alpha$  and  $\delta$  in mas. See Table 1 for contour levels, synthesized beam sizes (bottom left in the figure), and peak flux densities. See Table 2 for component parametrization.

Our model fit results do not show any evidence of backwards motion in the jet, in contrast to what was reported for components XB and XC at 8.4 GHz (Paper I; also for XD, XE, and XF, without counterparts at 15.4 GHz). As noted in Paper I, such apparently contracting motion

could be related to changes in the core region, e.g., the emergence of a component can induce, in its early stage of ejection, an apparent backwards motion of the rest of the jet components at cm wavelengths (e.g., Marcaide et al. 1985, Guirado et al. 1998, Ros et al. 1999). Our model fit also did not show the counterpart for component XB seen in 1999.41, at  $r \approx 0.4$  mas of the core. We tried to set an upper limit to the position of such a component in our first epoch, 1999.57, by forcing a model fit of the core with two components. Although we managed to model the core with two components, the model fit was no better, and therefore we found that a second component is not needed to explain the emission from the core. We suggest that if a second such component does exist, it should have stayed at roughly the same distance ( $\approx 0.2$  mas) at both epochs, and with an estimated uncertainty in its flux density of 100%.

The 15.4 GHz total flux density of QSO 1039+811 decreased by 12% between 1999.57 and 2000.46, changing from  $(926 \pm 2)$  mJy down to  $(826 \pm 3)$  mJy, which corresponds to a monochromatic luminosity of  $L_{15 \text{ GHz}} = (7.4 \text{ to } 8.3) \times 10^{38}$  W. The flux decrease is mainly due to the decrease in flux density of UA, from  $(883 \pm 2)$  mJy to  $(785 \pm 2)$  mJy (11% change). Assuming that the 8.4 GHz flux density of the source did not change between 1999.41 and 1999.57, we obtain  $\alpha = 0.08$ , a flat spectrum for the milliarcsecond structure of QSO 1039+811. The inverted spectrum of component UA ( $\alpha_{\text{UA/XA}} = 0.34$ ) supports our suggestion that this component is the core.

### 3.9. QSO 1150+812

Our 15.4 GHz VLBA maps of QSO 1150+812 (Fig. 10,  $z=1.250$ ) show a one-sided core-jet structure directed southwards up to 4 mas ( $27 h^{-1}$  pc) from the core. There is also a hint for very faint emission extending up to about 5 mas, as our previous 8.4 GHz VLBA observations clearly confirm (Paper I). The 15.4 GHz total flux density of QSO 1150+812 slightly decreased from 946 mJy in 1999.57 down to 907 mJy in 2000.46 (4% change). Its monochromatic luminosity is  $L_{15 \text{ GHz}} \approx (8.0 \text{ to } 8.3) \times 10^{38}$  W, almost the same as the luminosity of QSO 1039+811, due to their very close values in redshift and flux density. Assuming that the 8.4 GHz flux density of the source did not change between 1999.41 and 1999.57, we obtain  $\alpha = -0.40$ , a moderately steep spectrum for the milliarcsecond structure of QSO 1150+812.

From the maps, there is no clear evidence of significant morphological changes in either the core or the jet structure. Nevertheless, our model fit does show such evidence. We modeled the source (Table 2) with six components at each observing epoch. The flux density of the brightest component, UA, decreased from 405 mJy in 1999.57 down to 355 mJy ( $\sim 12\%$ ) in 2000.46, yielding  $\delta_{\text{min}} \approx 2.1$  to 3.8. The ratio  $Q$  decreased from 1.46 in 1999.57 to 1.39

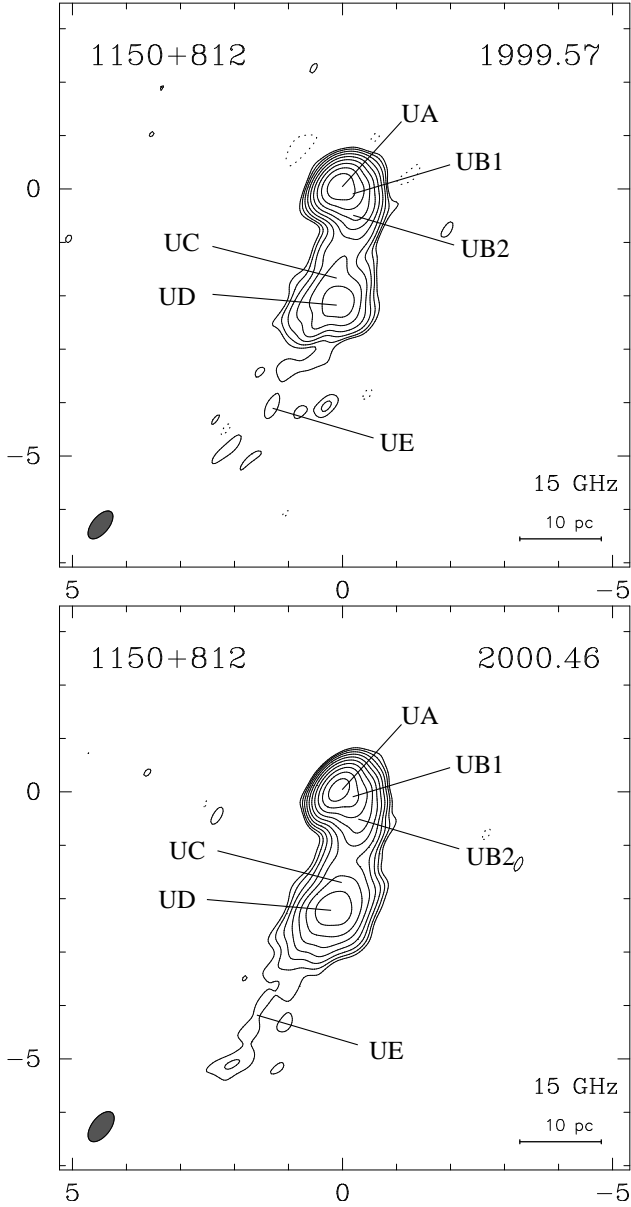


**Fig. 10.** VLBA images of QSO 1150+812 from observations on 27 July 1999 (1999.57) and 15 June 2000 (2000.46). Axes are relative  $\alpha$  and  $\delta$  in mas. See Table 1 for contour levels, synthesized beam sizes (bottom left in the maps), and peak flux densities. See Table 2 for component parametrization.

in 2000.46. We detected component UB1 at a distance of  $r \approx 0.33$  at an angle of  $\theta = (235^\circ \pm 5^\circ)$  at both epochs. Component UB2 is at a distance  $r \approx 0.65$  mas to 0.74 mas at an angle of  $220^\circ$  at both epochs. We suggest that component XB in Paper I, at distance  $r \approx 0.5$  mas, is a blend of components UB1 and UB2. UB2 seems to trace the curving of the jet, changing from an angle of  $235^\circ$  (component UB1) to a value of  $170^\circ$ , as displayed by the southern components of the jet. Component UC seems to correspond to XC in Paper I. We obtain  $\alpha_{UC/XC} = -1.53$ , if

UC and XC correspond to the same physical feature of the jet. The increase in flux density for this component is 28% between 1999.57 and 2000.46. Component UD is at a distance  $r = (2.25 \pm 0.05)$  mas at an angle  $\theta = 175^\circ \pm 5^\circ$ . Very similar values of  $r$  and  $\theta$  are found for XC (Paper I). Its flux density remained very stable.

### 3.10. BL 1749+701

The 15.4 GHz VLBA observations of BL 1749+701 (Fig. 11;  $z=0.770$ ) show a core-jet structure directed to the west/northwest that extends up to 4 mas. We identify in the images up to seven Gaussian components (Table 2). In all images, the central region (UA+UB) contributes 70% to 80% of the total radio flux. This region extends up to a distance of 0.4 mas ( $2.5 h^{-1} pc$ ), and we tentatively identify the brightest component, UA, with the core. The rest of the components, UC through UE, correspond to the jet, which extends up to  $r \approx 4$  mas ( $25 h^{-1} pc$ ). UC, at a distance of  $(1.15 \pm 0.15)$  mas, is likely the base of the jet. The jet is oriented to the west/northwest at an angle  $-69^\circ \pm 9^\circ$  for the inner 2.5 mas ( $16 h^{-1} pc$ ; components UC and UD), and then changes its direction northwards ( $\theta = -55^\circ \pm 3^\circ$ ) around a distance of  $(3.0 \pm 0.2)$  mas, keeping this orientation until the radio jet fades away.

The 15.4 GHz total flux density of BL 1749+701 oscillated around a mean value of 416 mJy between 1999.39 and 2000.99 (19 months), with variations usually not exceeding 7%. The corresponding monochromatic luminosity is  $L_{15 GHz} \approx (1.2 \text{ to } 1.3) \times 10^{38} W$ . The ratio of the core (taken as UA+UB) to the extended emission,  $Q$ , increased with time as follows: 2.4 (1999.39), 2.6 (1999.57), 2.9 (1999.85), 3.9 (2000.46), and 4.6 (2000.99), in agreement with the increasing activity of the core region. Assuming that the 8.4 GHz total flux density of the source did not change between 1999.39 and 1999.41 (one week), we obtain  $\alpha=0.0$ , showing a perfect flat spectrum for the source. The spectral index of component UA/XA is  $\alpha_{UA/XA} = 0.19$ , an inverted spectrum, which supports the suggestion that this is the core of the source.

Our previous 8.4 GHz VLBA observations of BL 1749+701 (Paper I) showed the existence of two components, XB and XC, at distances of  $(0.45 \pm 0.05)$  mas and  $(1.2 \pm 0.1)$  mas of the core (at P.A.  $\approx 60^\circ$ ), respectively. Component UB, at a distance of  $(0.3 \pm 0.1)$  mas, likely corresponds to XB. Similarly, component UC1, at  $(1.15 \pm 0.15)$  mas, is likely the counterpart of XC. In addition, we find another component between XC and XD, which we labeled UC2, at a distance of  $(1.6 \pm 0.2)$  mas from the core. This component is seen in the first three epochs (1999.39 through 1999.85), but was not detected later. This behaviour points towards real morphological changes in the inner  $10 h^{-1} pc$  of BL 1749+701, most likely the ejection and passage of components from the core. Components UD and UE belong to the weak, ex-

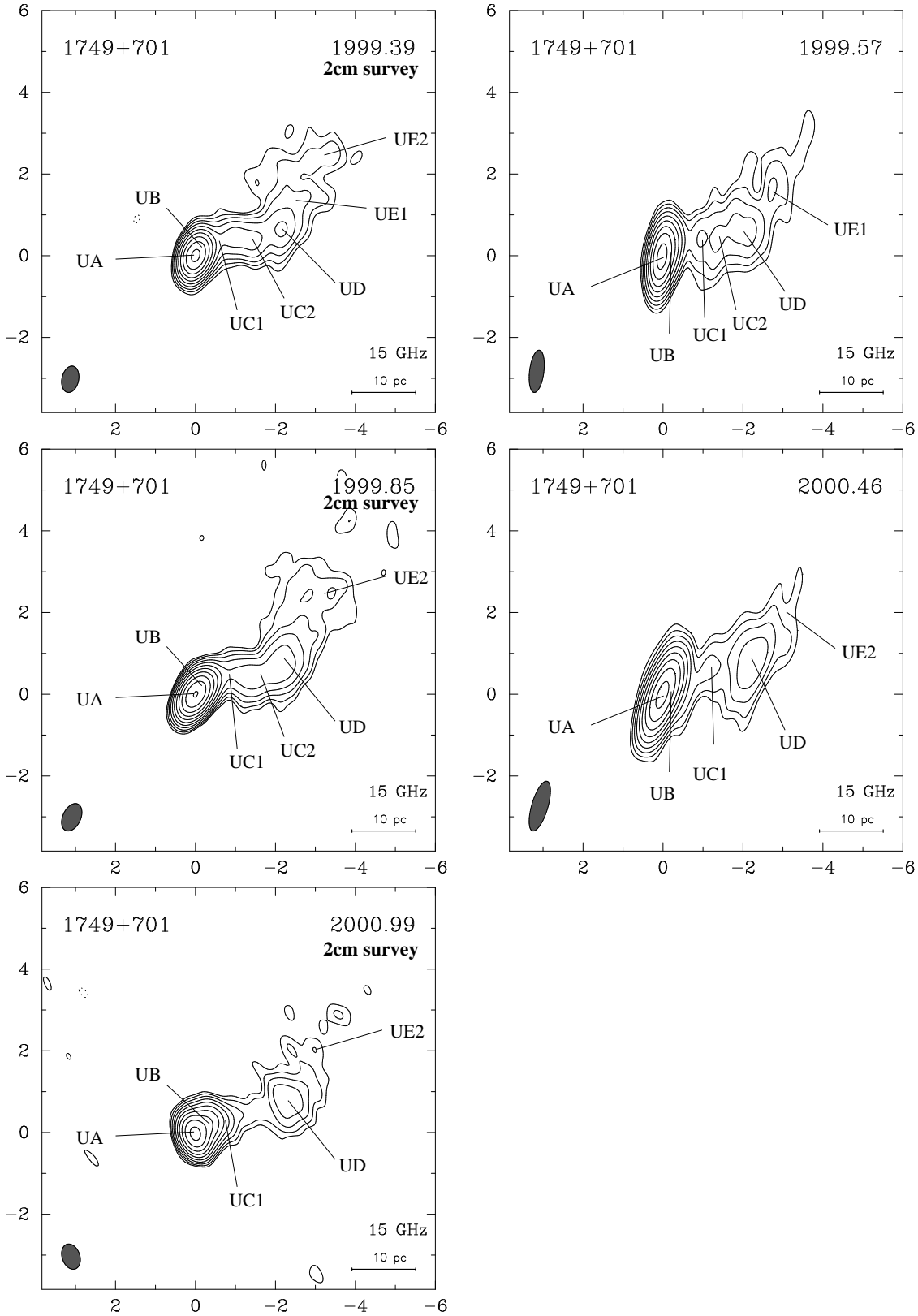


**Fig. 11.** VLBA images of BL 1749+701 from observations on 21 May 1999 (1999.39), 27 July 1999 (1999.57), 6 November 1999 (1999.85), 15 June 2000 (2000.46), and 28 December 2000 (2000.99). See Tables 1–3 for contour levels, beam sizes (bottom left in the maps), peak flux densities, and component parametrization. Axes are relative  $\alpha$  and  $\delta$  in mas.



tended jet. We identified UD with component XD (Paper I), based on their similar coordinates. Our model fit shows evidence for significant proper motions of components UB and UD, and of marginal significance for UC2 (see Table 4). The apparent proper motion of component UD coincides with the reported separation rate by Gabuzda et al. (1992) for their component K2. We hope to unambiguously confirm or rule out the existence of this proper motion from our astrometric analysis. Component XE (Paper I) could be a blend of two components, namely UE1 and UE2. At the position of UE1 the jet suddenly changes its direction of propagation, towards the north ( $r=(3.0\pm 0.2)$  mas;  $\theta \approx -58^\circ$ ). In our 15.4 GHz observations of 1999.57, this component seems to correspond to XE (epoch 1997.93; Paper I). We fail, however, to fit this component at epochs later than 1999.57. Our model fit shows a backwards superluminal motion for component UE2 (Table 4). We are skeptical about this motion, given the strong flux and morphological variability of the source beyond component UD. We do not detect any emission above  $3\sigma$  at angular distances  $\gtrsim 4.0$  mas from the core, implying a spectral index  $\alpha_{UF/XF} = -(2.1 \text{ to } 3.5)$ .

### 3.11. QSO 1803+784

The 15.4 GHz VLBA maps of QSO 1803+784 (Fig. 12;  $z=0.680$ , Véron-Cetty & Véron [2003]) reveal the same basic emitting structure seen at 8.4 GHz (Paper I); a one-sided core-jet oriented westward (P.A.  $\approx -90^\circ$ ). (Note that 1803+784 has been previously classified as a BL Lac object, but is now considered to be a QSO [Véron-Cetty & Véron 2003]). There are, however, significantly different features that appear in our model fit (Table 2), compared to our 8.4 GHz observations. We characterize reasonably well the source with six components, instead of the eight needed at 8.4 GHz, because of significant absorption at 15.4 GHz of the jet emission at  $r \gtrsim 4$  mas (we barely detect emission above  $3\sigma$ , which cannot be adequately model fitted). From our model fits, it follows that the inner 0.8 mas ( $4.9 h^{-1}$  pc) structure needs at least three components (UA, UB1, and UB2) to describe this region adequately describe this region, in contrast with the two components found at 8.4 GHz (XA and XB). We identify the brightest component, UA (likely the core), with component XA. Components UB1 and UB2 indicate the transition of the core to the jet region, and we suggest that component XB could be a blend of the two components seen at 15.4 GHz. The source structure at  $r \gtrsim 1$  mas is well characterized at 15.4 GHz by three components, UC, UD, and UE. Whilst the positions of UC and UD agree well with those of XC and XD, respectively (Paper I), we did not find clear counterparts for component XE, –at least for the first three epochs– nor for XF, XG, and XH.

The 15.4 GHz total flux density of QSO 1803+784 changed significantly from epoch to epoch (up to 26 %

between 1988.84 and 1999.57). Its monochromatic luminosity is  $L_{15\text{ GHz}} \approx (5.3 \text{ to } 6.6) \times 10^{38}$  W. The innermost regions of QSO 1803+784 ( $r \lesssim 1$  mas, equivalent to a linear distance of  $6.4 h^{-1}$  pc) encompass components UA, UB1, and UB2. The contribution of this innermost region to the total flux density amounts to 80% to 94%, depending on the epoch. (If we include component UC/XC, then the above figures become 93% to 98%, in agreement with the percentages reported in Paper I.) The total flux density variability of QSO 1803+784 closely follows that of the brightest component, UA, and is also partially modulated by fluctuations in the flux density of UB1 and UB2. The ratio of the core (taken as UA+UB1) to the extended emission,  $Q$ , confirms that the activity of QSO 1803+784 is core-dominated: 3.3 (1998.84), 5.2 (1999.57), 4.1 (1999.85), and 3.3 (2000.46).

Assuming that the 15.4 GHz total VLBI flux density of the source did not vary noticeably between 1999.41 and 1999.57, we obtain  $\alpha=0.41$ , a rather inverted spectrum for the milliarcsecond structure of QSO 1803+784. Similarly, we obtain the following indices for each component:  $\alpha_{UA/XA}=0.39$ ,  $\alpha_{(UB1+UB2)/XB}=1.0$ ,  $\alpha_{UC/XC}=-0.04$ ,  $\alpha_{UD/XD} \approx -0.70$ , and  $\alpha_{UE/XE} \approx 0.52$ . The spectral indices of UA and UB correspond with those expected for the innermost regions of the core, and those of UC and UD with what is expected in the inner-to-outer jet region. The value of  $\alpha_{UE/XE}$  is not expected for an optically thin component. While the non-simultaneity of the 8.4 GHz and 15.4 GHz could have some effect, it could also be that our component UE is indeed the result of the blending of XE and XF, in which case we obtain  $\alpha_{UE/(XE+XF)} \approx -0.63$ , a more typical value for an extended jet component. Our non-detection of significant emission around the positions of components XG and XH allows us to set upper limits for the spectral indices of these components ( $5\sigma$ ):  $\alpha_{UG/XG} \lesssim -2.6$ , and  $\alpha_{UH/XH} \lesssim -2.4$ .

The study of this source by VLBI is likely to give us relevant information on the kinematics and morphological changes of their innermost regions. The dramatic flux density variations displayed by the innermost regions of QSO 1803+784 along with the identification of a complex structure close to the core point to a possible ejection of components from the central engine. Another remarkable aspect of QSO 1803+784 is the stationarity of a component at  $(1.3\pm 0.1)$  mas. Schalinski (1990) suggested the existence of such a (stationary) component at 1.2 mas from the core. Krichbaum et al. (1993, 1994) used 43 GHz VLBI observations to show the existence of traveling components between the core and this component, setting it at a distance of 1.4 mas from the core. Both our 15.4 GHz and 8.4 GHz observations show this component (UC/XC) to be at  $(1.45\pm 0.05)$  mas, and no sign of any component at 1.2 mas existed between 1998.84 and 2000.46. We therefore

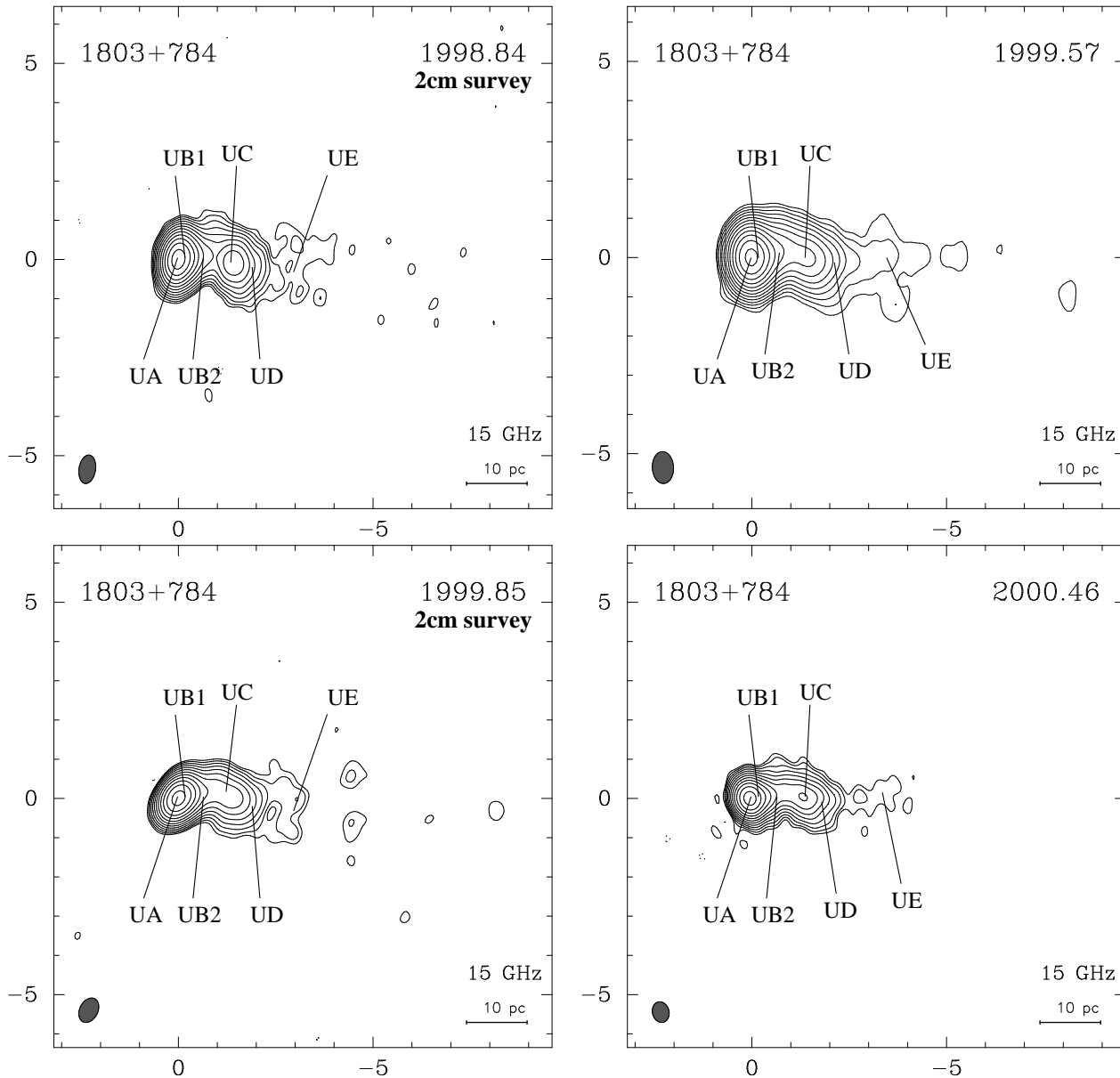


**Fig. 12.** VLBA Images of QSO 1803+784 from observations on 1 November 1998 (1998.84), 27 July 1999 (1999.57), 6 November 1999 (1999.85), and 15 June 2000 (2000.46). See Tables 1–3 for contour levels, beam sizes (bottom left in the maps), peak flux densities, and component parametrization. Axes are relative  $\alpha$  and  $\delta$  in mas.

suggest that there does indeed exist a stationary component at  $\approx 1.4$  mas ( $9 h^{-1}$  pc) from the core.

### 3.12. QSO 1928+738 (4C 73.18)

QSO 1928+738 (Fig. 13,  $z=0.3021$ ) is the most extensively studied radio source of the complete S5 polar cap sample, and the one that shows the richest structure. Our 15.4 GHz VLBA maps display a core-jet structure, with the jet southward-oriented (at an angle of  $160^\circ$ ), and extending up to 11.5 mas ( $49 h^{-1}$  pc). The 15.4 GHz total flux density of QSO 1928+738 decreased from 3006 mJy down

to 2889 mJy (4% change). Assuming that the 8.4 GHz flux density of the source did not vary significantly between 1999.41 and 1999.57, we obtain  $\alpha=0.02$ , a remarkably flat spectrum for the milliarcsecond structure of QSO 1928+738. We fitted reasonably well the brightness radio structure of QSO 1928+738 with nine components (Table 2). We model the innermost region ( $r \lesssim 1$  mas, corresponding to a linear distance of  $4.3 h^{-1}$  pc), with three components: UA, UB1, and UB2. Component UC ( $r=1.2$  mas at P.A.= $152^\circ$ ) indicates the transition from the innermost to the outermost structure of the jet.

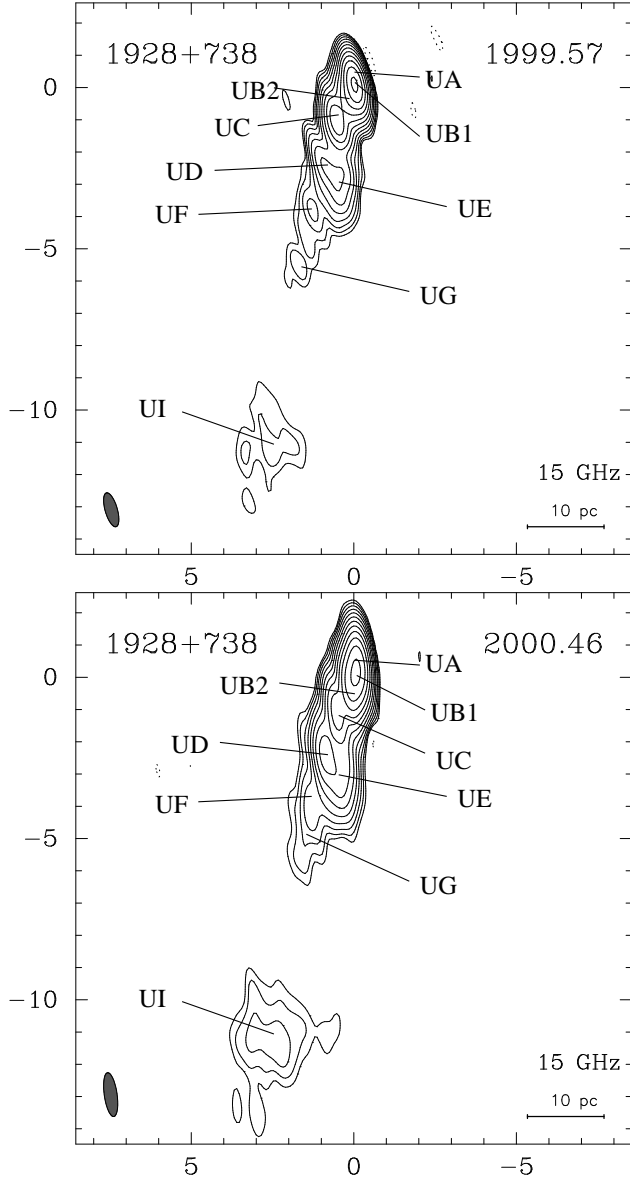


**Fig. 13.** VLBA images of QSO 1928+738 (4C 73.18) from observations on 27 July 1999 (1999.57) and 15 June 2000 (2000.46). Axes are relative  $\alpha$  and  $\delta$  in mas. See Table 1 for contour levels, synthesized beam sizes (bottom left in the maps), and peak flux densities. See Table 2 for component parametrization.

UA, the brightest component of QSO 1928+738 at both epochs, is not at the origin of coordinates, but to the north at  $r=(0.35\pm 0.05)$  mas from the origin, at an angle of  $-18^\circ\pm 2^\circ$ . Component UB1 is at the origin, and component UB2 is at  $r=(0.35\pm 0.05)$  mas at an angle of  $145^\circ\pm 5^\circ$ . The total intensity emission is dominated by this innermost region. Indeed, the combined emission from components UA, UB1, and UB2 amounts to 71% (70%) of the total at the first (second) epoch. The inclusion of the closest jet components up to a distance of 3 mas increases

those figures to 96% and 94% on 1999.57 and 2000.46, respectively. The ratio of the emission from the core region (taken here as UA+UB1) to the extended emission was  $Q=1.1$  in 1999.57, and  $Q=0.9$  in 2000.46. Although the compactness of the source is thus moderate, the overall source activity seems to be driven by the core, as the total flux density closely follows the core behaviour.

The spectral index of the innermost component, UA, is  $\alpha_{UA/XA}=0.04$ , as one would expect if UA were the core. Note that though the total intensity of QSO 1928+738 only varied by 4% between 1999.57 and 2000.46, the flux density of each component varied much more strongly. The decrease in flux density of UA, together with its change in position (a shift of 0.13 mas northward), could indicate that a component was ejected around or before 1999.57. Assuming this is the case, our model fit for UA at the second epoch suggests that the core is at least 0.4 mas to the north of component UB1, in agreement with previous estimates (e.g., Guirado et al. 1998, Ros et al. 1999).

Component XC (Paper I) is likely a blend of components UB2 and UC. As mentioned earlier, component UC is a signpost in the inner-to-intermediate structure of the jet. From this position onwards, the jet displays a noticeable change in its direction, from  $150^\circ$  at  $r=1.25\pm 0.05$  mas (UC) to  $160^\circ$  at  $r=2.55\pm 0.05$  mas (UD). Component UE at  $r=3.05\pm 0.05$  mas at  $\theta=173^\circ$ , shows a sudden change in the main orientation of the jet, which at the distance of component UF ( $r=3.95\pm 0.05$  mas) recovers its initial orientation ( $\theta=162^\circ\pm 2^\circ$ ). Component UG ( $r=5.45\pm 0.15$  mas;  $\theta=166^\circ\pm 2^\circ$ ) signals a first termination of the jet at a linear distance of  $25 h^{-1}$  pc. The 15.4 GHz jet reappears at almost twice that distance ( $r=11.55\pm 0.05$  mas, corresponding to  $50 h^{-1}$  pc, at an angle of  $167^\circ$ ). We identify this component, UI, with component XI (Paper I), which is found at essentially the same distance and angle, and suggests it is a stationary component of the jet. The extended jet structure of QSO 1928+738 at 8.4 GHz (Paper I) is richer in components than the one seen at 15.4 GHz. In particular, we fail to detect any significant emission beyond component UI ( $r=11.6$  mas), while the 8.4 GHz VLBA jet extends at least out to  $(25\pm 1)$  mas.

The activity of QSO 1928+738 is so intense that the task of identifying components from VLBI observations taken at different epochs and frequencies becomes challenging. For example, the astrometric studies carried out by Guirado et al. (1998) and Ros et al. (1999) indicated that the core position of QSO 1928+738 is to the north of the reference point chosen in earlier works. Ros et al. (1999) estimated the offset between the true core position and their 8.4 GHz observations to be about 1.5 mas to 2 mas. Our previous 8.4 GHz observations (Paper I) showed component XA to be at  $r=0.65\pm 0.15$  mas northward. The shift we find for its counterpart at 15.4 GHz, UA, is, however, significantly smaller

( $r = 0.35 \pm 0.05$  mas). If, as Guirado et al. and Ros et al. suggested, the “true” core is very much self-absorbed, we should expect to see a 15.4 GHz VLBI component northward of the 8.4 GHz component detected in Paper I (i.e., UA northward of XA). We fail, however, to detect such a component. A likely explanation is the potential confusion in the identification of components at 8.4 GHz and 15.4 GHz, despite our relatively close campaigns in 1999.

Another remarkable point is the proper motion of components in the jet of QSO 1928+738. Ros et al. (1999) reported a mean proper motion of  $(0.32 \pm 0.10)$  mas/yr for components in the inner 2.5 mas of the jet. Our model fit for the innermost regions of QSO 1928+738 does not, at this stage, show evidence for such large motions. Murphy et al. (2003) have recently reported a wide range of proper motions in QSO 1928+738, from nearly stationary ( $0.02$  mas/yr or  $0.5 c$ ) to relatively fast ( $0.82$  mas/yr or  $19 c$ ), based on VSOP observations. Unfortunately, there is no reference in their work to make it possible to identify which regions show superluminal motions. The authors mention that their model fitting shows that a relativistic, variable speed-ejecta ballistic model is preferred over a relativistic helical-jet model. If this is the case, then it is no surprise that component identification is so difficult for the source, especially if observations are widely spaced in time. Our quasi-simultaneous VLBA observations at 15.4 GHz and 43 GHz will shed light on the above two controversial issues (component identification and proper motion), and might be very useful in setting stringent limits on the putative core position.

### 3.13. BL 2007+777

Our VLBA maps of BL 2007+777 (Fig. 14,  $z=0.342$ ) display a one-sided core-jet structure oriented westward. The jet extends up to 6.9 mas ( $31 h^{-1}$  pc). The 15.4 GHz total flux density of BL 2007+777 seems to have steadily increased between 1999.57 and 2000.46, from 825 mJy up to 1258 mJy (52%). From then on, the source started to fade down to 948 mJy in 2001.17, corresponding to a decrease of 25% in less than nine months. Its monochromatic luminosity is quite modest ( $L_{15.4 \text{ GHz}} \approx (4.3 \text{ to } 6.6) \times 10^{37}$  W); it is the least powerful source after BL 0454+844.

We fitted its brightness radio structure with six components at all epochs except 2000.46, where only five components were model fitted (Table 2). We need up to four components (UA1, UA2, UB1, and UB2) to adequately describe the inner 1-mas region ( $4.6 h^{-1}$  pc). In contrast, the modeling of this region at 8.4 GHz required only two components, one at the origin (XA), and a second one at  $r = 0.55 \pm 0.05$  mas (XB). The brightest 15.4 GHz component at all epochs is UA1, which is not at the origin, but shifted  $0.3 \pm 0.1$  mas eastward. This component went undetected at 8.4 GHz (Paper I). If this finding is confirmed by our 43 GHz observations, we have another case, along with

those of QSO 0212+735 and QSO 1928+738, in which the core position is shifted from the reference point normally used, the peak-of-brightness. Component UA2 is at the origin, component UB1 is at  $r=0.35 \pm 0.05$  mas at angle  $-85^\circ$ , and component UB2 is at  $r=0.85 \pm 0.25$  mas at angle  $-83^\circ \pm 7^\circ$ . Our model fit shows a significant proper motion for component UB1, and marginally significant ones for UA1, UC, and UF (Table 4). The model fitting procedure merged UB1 and UB2 into just one component in 2000.46. Note that the flux density of UB1 in 2000.46 is more than 50% greater than at the other three epochs, and close to the common flux of UB1+UB2 in the closest epochs. Hence we suggest that the motion of an undetected component, probably traveling from UA2 toward UC (and passing through UB1), could be responsible for the blending. This could, in turn, explain the apparent paradox of a forward superluminal motion of UB1, and a backward one for UC. The ratio  $Q$  of the emission from the core region (taken as UA1+UA2) to the extended emission shows a moderate dominance of the core which modulates the overall emission: 1.59 (1999.57), 1.63 (1999.85), 1.71 (2000.46), and 1.21 (2001.17). The total intensity emission is strongly dominated by that of the innermost region (the inner  $5 h^{-1}$  pc). Indeed, the combined emission from components UA1, UA2, UB1, and UB2 amounts to 90% of the total at both epochs. Component UC contributes 3% to 9%, and component UF 2% to 5%. Assuming that the 8.4 GHz flux density of the milliarcsecond structure of BL 2007+777 did not change appreciably between 1999.41 and 1999.57, we obtain  $\alpha = -0.16$ , a moderately steep spectrum. Despite the non-varying global contribution to the flux density from the inner 1 mas structure of BL 2007+777, significant flux density variations do exist for each component.

Component UC, at a distance of  $1.28 \pm 0.10$  mas at P.A.  $-92^\circ \pm 5^\circ$  is likely to correspond to component XC in Paper I. We fail, however, to see any clear counterpart to component XD ( $r = 1.65 \pm 0.05$  mas at angle  $-92^\circ \pm 6^\circ$ ; Paper I). We encounter a similar situation with respect to component XE ( $r = 4.75 \pm 0.05$  mas at  $-100^\circ$ ), for which we only find a clear counterpart in our last epoch (UE, at  $r \approx 5.1$  mas at P.A.  $\approx -106^\circ$ ). This component indicates a curvature in the jet of BL 2007+777, as confirmed by our previous 8.4 GHz VLBA observations (paper I), and VSOP observations at 5 GHz (Peng et al. 2000, Jin et al. 2001). From the images, there are hints for the existence of component UE at the other epochs, with marginal detections just above  $3\sigma$ , but which our model fit failed to reproduce. If real, the inferred spectral index is  $\alpha_{\text{UE/XE}} \lesssim -1.9$ . The 15.4 GHz jet reappears at an angular distance of  $r = 6.5 \pm 0.4$  mas, at an angle of  $\approx -95^\circ$  (component UF). The similar component at 8.4 GHz (XF in Paper I), is at  $r \approx 6.7$  mas, which agrees relatively well. In the maps, there seems to be more than just one, albeit weak, component around 6 mas to 7 mas

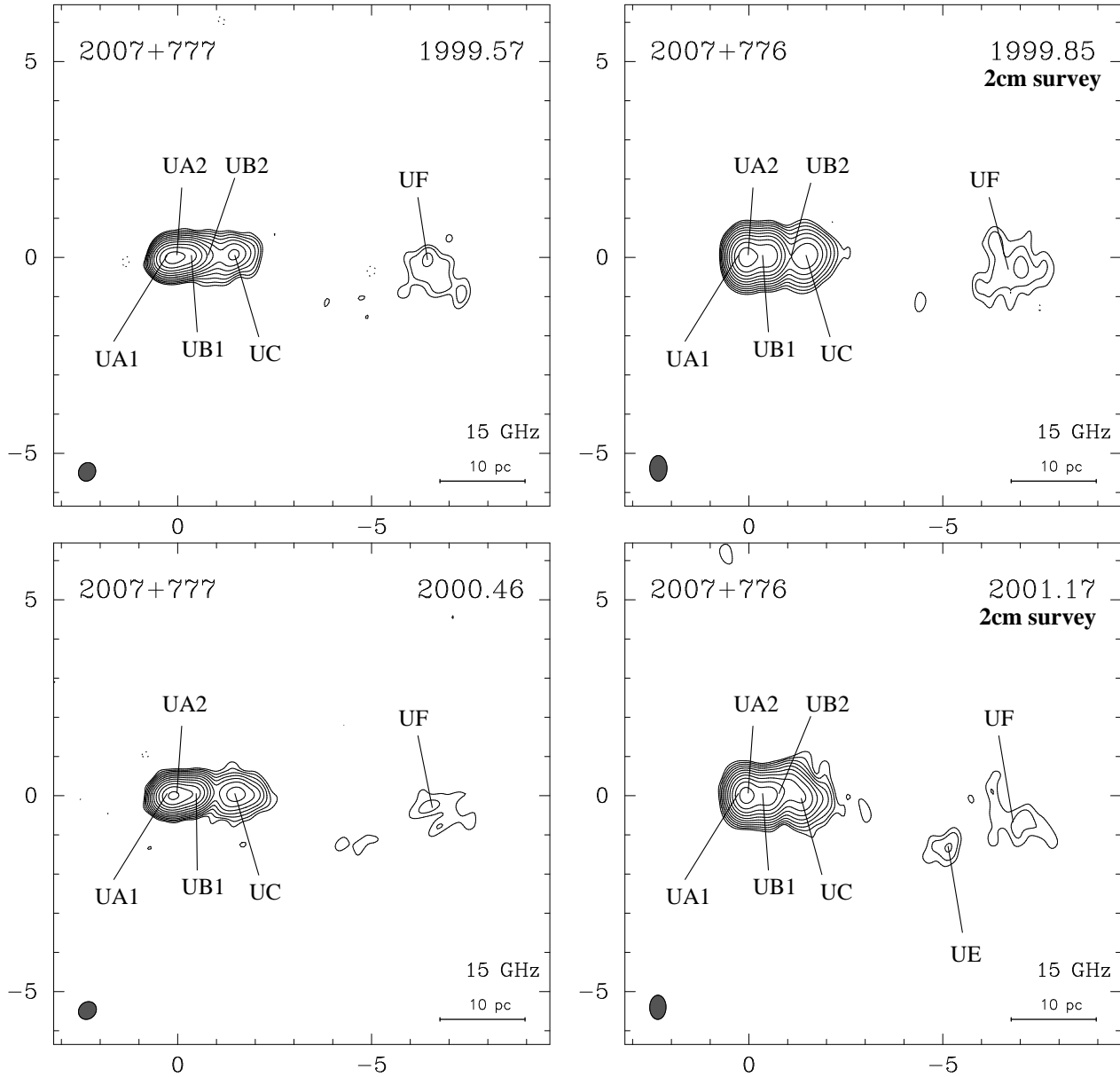


**Fig. 14.** VLBA images of BL 2007+777 from observations on 27 July 1999 (1999.57), 6 November 1999 (1999.85), 15 June 2000 (2000.46), and 4 March 2001 (2001.17). See Tables 1–3 for contour levels, beam sizes (bottom left in the maps), peak flux densities, and component parametrization. Axes are relative  $\alpha$  and  $\delta$  in mas.

westward. Although the model fit could not confirm our suspicion, we suggest UF is the blending of at least two sub-components, which would explain the large variations we find in its radial coordinate.

Our non-detection of a component around 1.7 mas to 2.0 mas might be somewhat uncomfortable, since this component seems to have been detected also by 5 GHz VSOP observations close to those reported in Paper I (Krichbaum et al. 2000). Although the use of these data (taken at different wavelengths and with different arrays) casts some doubts on their identification, we propose the following explanation: Component UA1 is the stationary

core of BL 2007+777, which lies at  $r \gtrsim 0.2$  mas to 0.4 mas eastward from the point normally used as reference. At lower frequencies, UA1 is not seen alone, but as a blended component (UA), at the origin. If we simply subtract the shift, the position of the “unseen” component would correspond with that of UC.

#### 4. Summary

We observed the thirteen extragalactic radio sources of the S5 polar cap sample at 15.4 GHz with the Very Long Baseline Array, on 27 July 1999 (1999.57) and 15 June

2000 (2000.46). We present the maps from those two epochs, along with maps obtained from observations of the 2 cm VLBA survey for some of the sources of the sample, making a total of 40 maps. Our observations correspond to the first two epochs at 15.4 GHz of a program directed to study the absolute kinematics of the radio source components of the members of the sample, by means of phase delay astrometry at 8.4 GHz, 15.4 GHz, and 43 GHz. We summarize our main findings from our VLBA imaging at 15.4 GHz of the sources of the complete sample as follows:

- All of the 13 radio sources display at 15.4 GHz prominent one-sided jet structures, except for QSO 0615+820. This source shows the most intriguing radio structure of all the sources of the sample, displaying a complex structure despite being the most compact QSO of the sample ( $l \lesssim 15.4 h^{-1} \text{ pc}$ ).
- The imaging at 15.4 GHz yielded a better resolved view of the sources, compared to our previous imaging at 8.4 GHz (Paper I). In this way, we were able to disentangle the inner milliarcsecond structure of some of the sources, thus resolving out components that appeared blended at 8.4 GHz. For most of the sources we identified the brightest feature in each radio source with the core. These identifications are supported by the spectral index estimates for those brightest features ( $\alpha$  ranges from 0.04 up to 1.99) except for QSO 0615+820, for which we find  $\alpha = -0.69$  for the apparent core of the source. Higher frequency observations might be of great help to disentangle the radio brightness structure of this challenging object. The putative core of QSO 1150+812 also shows a moderately steep spectrum ( $\alpha \approx -0.13$ ).
- The sources cover a wide range of luminosity values that spans almost four orders of magnitude: from the least luminous object, BL 0454+844 ( $L_{15 \text{ GHz}} \approx (0.6 \text{ to } 1.3) \times 10^{36} \text{ W}$ ), up to the most luminous one, QSO 0212+735, with a monochromatic luminosity of  $L_{15 \text{ GHz}} = (9.25 \pm 0.05) \times 10^{39} \text{ W}$ . The luminosity of QSO 0212+735 is so impressive that its weakest component (UG, at the not less impressive distance of  $85 h^{-1} \text{ pc}$  from the core) has  $L_{15 \text{ GHz}} \approx 1.2 \times 10^{38} \text{ W}$ , about 100 times more powerful than BL 0454+844, and competes in power with several other sources of the complete sample.
- Most of the sources show core-dominance in the overall emission, as given by the core-to-extended ratio,  $Q$ . Indeed,  $Q$  is significantly greater than unity for most sources and epochs. Nevertheless, there is a large spread in the values of  $Q$ , indicating a corresponding spread in the core dominance. The four sources with the largest core dominance are BL 0716+714 ( $Q = 6$  to 22), QSO 1039+811 ( $Q = 19$  to 21), for BL 0454+844 ( $Q = 9$  to 16), and QSO 0016+731 ( $Q = 4$  to 11). The rest of the sources show moderate-to-large core dom-

inance, with values in the range 1.3 to 5.2. The two sources with the lowest  $Q$  values are QSO 0212+735 ( $Q = 0.8$  to 1.0) and QSO 0615+820 ( $Q = 0.9$  to 1.4). While QSO 0212+735 has a low value due to the emission strength of its innermost jet structure, the case of QSO 0615+820 is slightly different. Here, the halo-like, albeit relatively compact, emission competes in strength with the component we tentatively identify with the core (UA1).

- Three of the sources have the most inverted spectrum component shifted with respect to the origin in the map, which approximately coincides with the peak-of-brightness at both 15.4 GHz and 8.4 GHz. At 15.4 GHz, the offsets of these inverted components are: QSO 0212+735,  $\Delta r = 0.6 \text{ mas}$ ; QSO 1928+738,  $\Delta r = 0.35 \pm 0.05 \text{ mas}$ ; BL 2007+777,  $\Delta r = 0.25 \pm 0.05 \text{ mas}$ . Our 8.4 GHz observations in 1999.41 (Paper I), close to our first 15.4 GHz observations (1999.57), also show offsets for QSO 0212+735 ( $\Delta r \approx 0.6 \text{ mas}$ ) and QSO 1928+738 ( $\Delta r \approx 0.5 \text{ mas}$ ), but not for BL 2007+777, whose peak-of-brightness coincides with the origin in the map. In the standard synchrotron self-absorption theory, the high-frequency components are closer to the central machine than the low-frequency ones. Within their positional uncertainties, we find that the source morphologies of those objects, as seen at 8.4 and 15.4 GHz, are satisfactorily explained by the standard scenario.

*Acknowledgements.* MAPT is supported by the Spanish National program Ramón y Cajal. We are very grateful to Alan Roy for a careful reading of our manuscript, and for his idiomatic and grammar corrections. We are also grateful to the 2cm VLBA survey team for kindly allowing us to use part of their data. This work has been partially financed by Grants AYA2001-2147-C02-01 and AYA2001-2147-C02-02 of the Spanish DGICYT, and by the European Grant IHP-MCFI-99-1. The NRAO is a facility of the National Science Foundation operated under cooperative agreement by Associated Universities, Inc. This research has made use of the NASA Astrophysics Data System.

## References

- Bach, U., Krichbaum, T. P., Ros et al. (astro-ph/0309404)  
 Eckart, A., Witzel, A., Biermann, P., et al. 1986, A&A, 182, 17  
 Eckart, A., Witzel, A., Biermann, P., et al. 1987, A&AS, 67, 121  
 Gabuzda, D. C., Cawthorne, T. V., Roberts, D. H., Wardle, J. F. C. 1992, AJ, 388, 40  
 Guirado, J. C., Marcaide, J. M., Ros, E., et al. 1998, A&A, 336, 385  
 Hummel, C. A., Schalinski, C. J., Krichbaum, T. P., Witzel, A., Johnston, K. J. 1988, A&A, 204, 68  
 Hummel, C. A., Krichbaum, T. P., Witzel, A., et al. 1997, A&A 324, 857

- Hummel, C. A., Krichbaum, T. P., Witzel, A., et al. 1997, *A&A*, 324, 857
- Lobanov, A.P., Krichbaum, T.P., Witzel, A., et al. 1998, *A&A*, 340, L60
- Peng, B, Kraus, A., Krichbaum, T. P., et al. 2000, *A&A*, 353, 937
- Jin, C., Krichbaum, T. P., Witzel, A., et al. 2001, *ApSS*, 278, 97
- Kellermann, K.I., Vermeuler, R.C., Zensus, J.A., & Cohen, M.H. 1998, *AJ*, 115, 1295
- Krichbaum, T. P., Witzel, A., Graham, D. A., Schalinski, C. J., Zensus, J. A. 1993. New Results from VLBI at 43 GHz. In *Sub-arcsecond Radio Astronomy*, ed. R. J. Davis, & R. S. Booth, (Melbourne: Cambridge University Press), 181
- Krichbaum, T.P., Witzel, A., Standke, K.J., et al. 1994. mm-VLBI: Bending of Jets in the Vicinity of AGN. In *Compact Extragalactic Radio sources*, ed. J. A. Zensus & K. I. Kellermann (Green Bank, WV: NRAO), 39
- Kühr, H., Witzel, A., Pauliny-Toth, I. I. K., Nauber, U. 1981, *A&AS*, 45, 367
- Marcaide, J. M., Bartel, N., Gorenstein, M.V., et al. 1985, *Nature*, 314, 424
- Murphy, D. W., Preston, R. A., Hirabayashi, H. 2003, *New Astron. Rev.*, 47, 633
- Otterbein, K., Krichbaum, T. P., Kraus, A., et al. 1998, *A&A*, 334, 489
- Pearson, T. J. 1991, *BAAS*, 23, 991
- Quirrenbach, A., Witzel, A., Wagner, S., et al. 1991, *ApJ*, 372, 71
- Ros, E., Marcaide, J. M., Guirado, J. C., et al. 1999, *A&A*, 348, 381
- Ros, E., Marcaide, J. M., Guirado, Pérez-Torres, M.A., 2001, *A&A*, 376, 1090
- Schalinski, C. J. 1990, Dissertation, Untersuchungen der Zentralregionen aktiver Galaxienkerne, Friedrich-Wilhelms-Universität zu Bonn, Germany
- Shepherd, M. C., Pearson, T. J., Taylor, G. B. 1994, *BAAS*, 26, 987
- Stocke, J.T. & Rector, T.A. 1997, *ApJ*, 489, L17
- Véron-Cetty, M.-P. & Véron, P. 2003, *A&A*, 412, 399
- Wagner, S. J., Witzel, A., Heidt, J., et al. 1996, *AJ*, 111, 2187
- Zensus, J.A., Ros, E., Kellermann, K.I., et al. 2002, *AJ*, 124, 662